

UCLA

UCLA Electronic Theses and Dissertations

Title

Mid-21st Century Changes to Surface Hydrology Over the Los Angeles Region

Permalink

<https://escholarship.org/uc/item/8zt5x06t>

Author

Schwartz, Marla Ann

Publication Date

2013

Peer reviewed|Thesis/dissertation

UNIVERSITY OF CALIFORNIA

Los Angeles

Mid- 21st Century Changes to Surface Hydrology

Over the Los Angeles Region

A thesis submitted in partial satisfaction
of the requirements for the degree Master of Science
in Atmospheric and Oceanic Sciences

by

Marla Ann Schwartz

2013

ABSTRACT OF THE THESIS

Mid- 21st Century Changes to Surface Hydrology
Over the Los Angeles Region

by

Marla Ann Schwartz

Master of Science in Atmospheric and Oceanic Sciences

University of California, Los Angeles, 2013

Professor Alex Hall, Chair

Abstract

This thesis explores projected mid-21st century changes to surface hydrological fluxes and states in the Los Angeles region at 2km resolution. This work quantifies and describes potential impacts of climate change to precipitation, runoff, evapotranspiration and soil column moisture content in the Los Angeles region. Little previous research has focused on the impacts of climate change to water resources and surface hydrology in this region. We simulate detailed climatologies of surface hydrology for the late 20th century and mid 21st century. By looking at differences between the future and baseline periods, mid-century changes to surface hydrology relative to the late 20th century can be evaluated in our study region.

Using dynamical downscaling techniques and the Weather Research and Forecasting (WRF) model, we develop a detailed high-resolution climatology for the Los Angeles region from coarse-resolution North America Regional Reanalysis (NARR) data and output from five

“business as usual” global climate model (GCMs) simulations in the Fifth Coupled Model Intercomparison Project (CMIP5) data archive. Output from the dynamical downscaling WRF simulations is then used to force the offline Noah Land Surface Model (Noah-LSM), which simulates near-surface state variables and surface turbulent fluxes. This methodology allows us to assess potential impacts of climate change to surface hydrology in the Los Angeles region at scales relevant to local policy makers or water resources planners.

The thesis of Marla Ann Schwartz is approved.

J. David Neelin

Glen MacDonald

Alex Hall, Chair

University of California, Los Angeles

2013

Table of Contents

1. Introduction

2. Methods

- 2.1. Description of the Noah Land Surface Model (Noah-LSM)
 - 2.1.1. Noah-LSM Development and Introduction
 - 2.1.2. Noah-LSM Forcing Input and Simulation Output
 - 2.1.3. Noah-LSM Physics
- 2.2. Noah-LSM Initializations
- 2.3. Meteorological Forcing Inputs for Noah-LSM simulations
 - 2.3.1. Global Climate Simulations
 - 2.3.2. WRF and Dynamical Downscaling Methods to Produce Noah-LSM Forcing Inputs

3. Validation

- 3.1. Evaluation data
 - 3.1.1. CIMIS Observation Stations
 - 3.1.2. USGS HCDN Streamflow Gauges
- 3.2. Validation of Noah-LSM Output
 - 3.2.1. Soil Temperature
 - 3.2.2. Evapotranspiration
 - 3.2.3. Runoff
- 3.3. Validation of dynamically downscaled WRF output used to force Noah-LSM simulations
- 3.4. Water budget closure

4. Results

- 4.1. Climatology of baseline surface hydrology
- 4.2. Changes to annual mean surface hydrological variables
 - 4.2.1. Precipitation
 - 4.2.2. Runoff
 - 4.2.3. Evapotranspiration and potential evapotranspiration
 - 4.2.4. Fractions of evaporation over precipitation and runoff over precipitation
 - 4.2.5. Soil column moisture content

5. Discussion and summary

6. References

List of Figures

1. Topography and resolution of our study domain
2. Noah-LSM model structure
3. WRF Simulation Domains
4. Locations of CIMIS weather stations used for model evaluation
5. Locations of USGS HCDN streamflow gauges used for model evaluation
6. Validation of variability of minimum daily soil temperature in Noah-LSM
7. Validation of variability of maximum daily soil temperature in Noah-LSM
8. Validation of variability of daily evapotranspiration in Noah-LSM
9. Validation of variability of runoff in Noah-LSM
10. Validation of variability of incoming daily solar radiation in WRF
11. Validation of baseline water budget closure in Noah-LSM
12. Validation of future water budget closure in Noah-LSM
13. Noah-LSM annual mean precipitation for the baseline period
14. Noah-LSM percentages of annual mean precipitation that a) results in runoff and b) is returned to the atmosphere through evapotranspiration for the baseline period.
15. Noah-LSM annual mean runoff for the baseline period
16. Noah-LSM annual mean evapotranspiration for the baseline period
17. Noah-LSM annual mean potential evapotranspiration for the baseline period
18. Noah-LSM annual mean total soil column moisture content for the baseline period
19. Noah-LSM change in annual mean precipitation for all GCMs
20. Noah-LSM ensemble mean change in annual precipitation
21. Noah-LSM change in annual mean runoff for all GCMs
22. Noah-LSM ensemble mean change in annual runoff
23. Noah-LSM ensemble mean change in annual potential evapotranspiration
24. Noah-LSM change in annual mean evapotranspiration for all GCMs
25. Noah-LSM ensemble mean change in annual evapotranspiration
26. Noah-LSM ensemble mean changes to percentages of annual mean precipitation that a) results in runoff and b) is returned to the atmosphere through evapotranspiration
27. Noah-LSM change in annual mean soil column moisture content for all GCMs

List of Tables

1. Name and characteristics of the CMIP5 GCMs used for WRF dynamical downscaling.

1 Introduction

Climate change has been observed both globally and in the western United States, mainly due to anthropogenic forcing (Intergovernmental Panel on Climate Change 2007; U. S. Global Change Research Program 2009). Observed climate-related changes include warmer near-surface air temperatures, changes to precipitation patterns and intensity, increased atmospheric water vapor, more severe weather extremes, more common and intense droughts and floods, reduced snowpack, earlier melting of the snowpack, shifting of the runoff timing, and a rise in sea level (IPCC 2007). These changes present challenges for water resources, energy supply and demand, public health, and ecosystems and the environment.

The global mean surface air temperature increased around $.74^{\circ}\text{C}$ between 1906-2002, and the rate of increase is accelerating, with stronger increases observed over land surfaces than the ocean (Trenberth et al. 2007). Climate models estimate that global mean temperatures may increase from 1.4°C to 5.8°C over the next 100 years (IPCC 2007). Increasing temperatures are expected to continue to impact regional precipitation patterns, snow accumulation and snowmelt, soil moisture storage, river runoff and water available for vegetation. Among the components of the water cycle, surface runoff is perhaps most important to society. The IPCC identified freshwater resources as vulnerable to climate change and stressed the research demand to model runoff and surface hydrology process at higher resolutions in land surface models (2007).

While surface runoff is important, the water cycle is heavily impacted by the process of evapotranspiration, which accounts for approximately 60% to 65% of global precipitation (Brutsaert, 2005). Evapotranspiration accounts for the sum two separate processes: evaporation, where water is lost as vapor from surface water bodies or the soil to the air, and transpiration, where water is lost as vapor to the air through a plant's stomata or leaves. The

processes of evaporation and transpiration are key to the nexus of the water, carbon and energy cycles.

The impact of climate change on the water flux between the land and atmosphere has received much attention as a climate change issue and focus due to the potential implications for water resources (Schimel et al. 1997; Cox et al. 2000). There appears to be little agreement on the sign and magnitude of both historical and projected evapotranspiration trends. Some studies conclude that actual evapotranspiration in the Northern Hemisphere steadily decreased throughout the end of the 20th century, contrary to the initial expectation that surface warming would increase evapotranspiration rates (Peterson et al. 1995; Golubev et al. 2001). Decreasing evapotranspiration rates may be explained by increases in cloudiness and atmospheric aerosol concentrations, as well as changes to solar irradiance and diurnal temperature ranges, which reduce energy availability at the surface for evapotranspiration (Roderick and Farquhar, 2002). Moreover, stilling of the winds due to changes in vegetation and roughness height may also play a role in decreasing evapotranspiration trends. Additionally, other studies suggest that increasing soil-moisture limitations in moisture-limited regions also contribute to the recent decline of evapotranspiration trends (Jung et al. 2010). Until now, debates and uncertainties revolve around the trends in regional evapotranspiration.

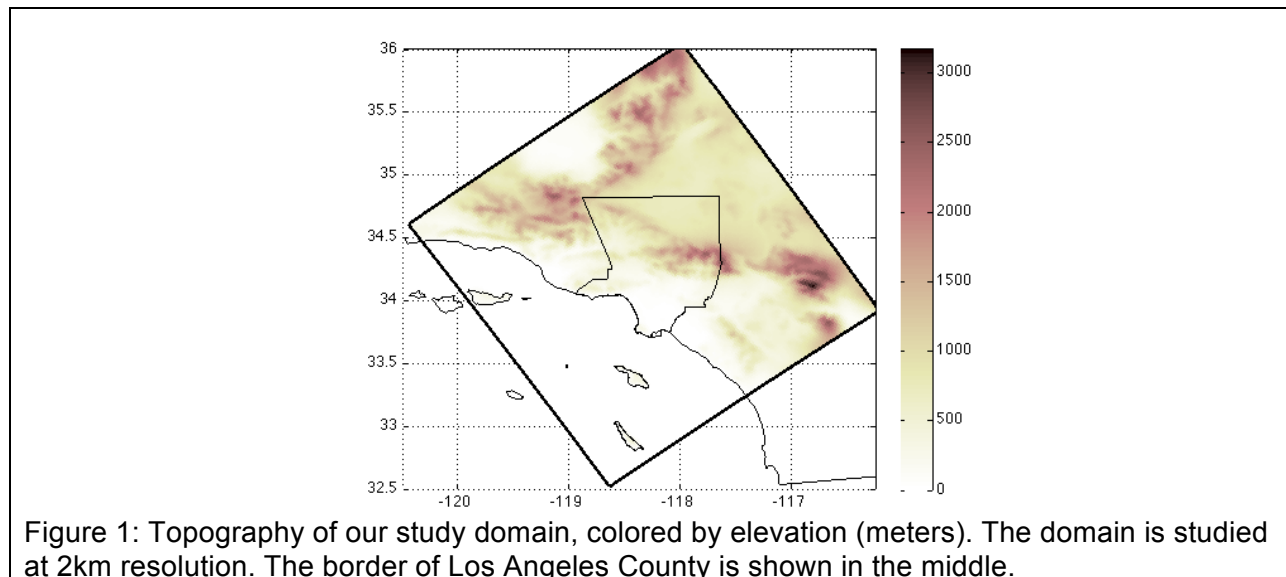
In addition to global studies on surface hydrology, previous research has focused on the impacts of climate change to water resources of the western United States (Dettinger and Cayan, 1995; Cayan 1996; Mote and Salathe, 2010). Results show that the snow water equivalent (SWE) measured on April 1st for the western United States has declined from 1950 to 2000, except in the southern Sierra Nevada Mountains of California (Mote 2003). Additionally, research shows that more winter precipitation fell as rain as opposed to snow during the period of 1949 to 2004 (Knowles et al. 2006). Moreover, earlier snowmelt runoff has been observed due to the earlier onset of spring (Dettinger and Cayan, 1995; Cayan et al. 2001; Stewart et al. 2004). In addition to research on the influence of climate change on the western United States,

much research has specifically examined the observed and projected influence of climate change on water resources and surface hydrology in Northern California's snow dominated regions (Gleick and Chalecki, 1999; Christensen et al., 2004; Hayhoe et al. 2004; Mote et al. 2005; Kapnick and Hall, 2010). However, few studies have evaluated the impacts of climate change to water resources and surface hydrology in the southern regions of California, particularly the Los Angeles region. Understanding the impact of climate change on surface hydrology and the partitioning of precipitation into runoff and evapotranspiration in the Los Angeles region is important for water resources planning.

The Los Angeles region is deeply dependent on numerous sources of water supply, both imported and natural. Imported resources for the Los Angeles region include water from the Colorado River, California State Water Project (from Northern California), and Los Angeles Aqueduct (from the Sierra Nevada Mountains). Additional sources include ground water, local reservoirs and desalination plants. Climate change is expected to impact Los Angeles' capability to store surface water due to changes to the location, intensity and frequency of precipitation. Any potential changes to surface hydrology or water resources in the Los Angeles region due to climate change will further strain a water system already heavily reliant on imported water; this will only obstruct efforts to make the Los Angeles region more sustainable and less vulnerable to climate change impacts. As such, it is important to examine adjustments to local surface hydrology so that resource managers, land use planners and policy makers can better prepare for the future. This requires very high-resolution information regarding the impact of future climate variability on surface hydrologic fluxes and states in the Los Angeles region.

The work of this thesis focuses on the Los Angeles region at 2km resolution. Figure 1 shows the border of our simulation domain, with the border of Los Angeles County shown in the middle. At such a high resolution, the main features of the domain's topography and coastlines are well represented. The Los Angeles region is characterized by a Mediterranean-type climate, with fairly drastic seasonal changes in rainfall and modest seasonal transitions in temperature.

Annual precipitation in the Los Angeles region ranges from approximately 100-1000 mm/year and the mean annual temperature ranges between 16°C and 18°C (Levien et al. 2002). Vegetation below 2000m is predominantly scrubs and chapparal, while vegetation above 2000m is mostly forest (Levien et al. 2002). The greater Los Angeles region is home a population of nearly 18 million people, who together account for nearly \$750 billion in economic activity every year (U.S. Metro Economies -- Gross Metropolitan). The rapidly growing metropolitan areas of the Los Angeles region already face issues of water stress, and any change to water resources will exacerbate this issue.



This study focuses on two three-year time periods: A “baseline” period (September 1, 1998-August 31, 2001) and a “future” period (September 1, 2058 – August 31, 2061). By looking at the differences between the future and baseline periods, mid 21st century climate change impacts to surface hydrology relative to the late 20th century can be evaluated for the Los Angeles region. Using the Noah Land Surface Model, we examine mid-21st century impacts to surface hydrology at 2km resolution in the Los Angeles region under a “business as usual” climate change signal from five global climate models (GCMs). We aim to assess the impact of future climate change on surface hydrologic fluxes and states in the Los Angeles region.

In this study, we refine our understanding of regional changes to surface hydrology. In section 2, we present the description of the configurations of the two models used in this work: the Noah Land Surface Model (Noah-LSM) and Weather Research and Forecasting Model (WRF). In section 3, we complete a validation of both models' abilities to simulate realistic surface hydrology and meteorological variability in our domain. In section 4, we present our results from Noah-LSM and assess mid-21st century changes to surface hydrology in the Los Angeles region. Finally, in section 5, we discuss the implications of our results and highlight the need for further research.

2 Methods

In this section, we describe the offline Noah Land Surface Model (Noah-LSM) we use to simulate surface and near-surface hydrology in the Los Angeles region. We also cover information regarding model initialization for the Noah-LSM simulations. Additionally, we describe the Weather and Research Forecasting (WRF) Model and dynamical downscaling methods used to simulate the meteorological forcing variables for our Noah-LSM simulations.

2.1 Description of the Noah Land Surface Model (Noah-LSM)

2.1.1 Noah-LSM Development and Introduction

The Noah (National Centers for Environmental Prediction, Oregon State University, Air Force, and Hydrologic Research Lab) Land Surface Model (LSM) is a community land surface model that simulates near-surface state variables and surface turbulent fluxes from eight meteorological forcing variables. From the time Noah-LSM was developed by Mahrt and Pan (1984), a series of modifications have been made to increase forecast accuracy and efficiency and to improve the simulation of various land surface processes. Noah-LSM is widely used in both operational weather forecasting and climate models; Noah-LSM has been used operationally since 1996 as the land surface model in regional and global climate models at the National Centers for Environmental Prediction (NCEP) and as the land component of the Weather Research and Forecasting model (WRF) at the National Center for Atmospheric Research (NCAR) (Wang et al 2010). Noah-LSM has also been used in land data assimilation systems, including the Land Information System (Peters-Lidard et al. 2007), the High Resolution Land Data Assimilation System (Chen et al. 2007), and the North American Land Data Assimilation System (Mitchell et al. 2004).

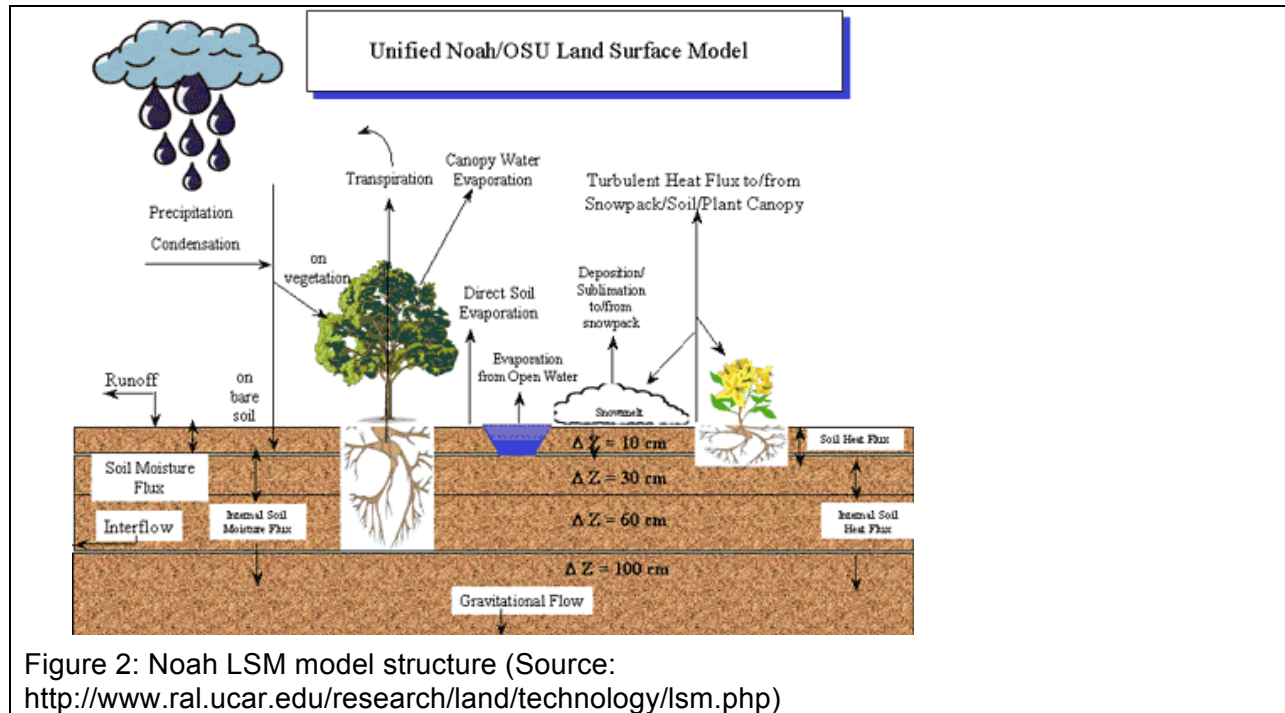
Noah-LSM can be run in either offline mode or coupled to a climate model. In the offline mode, Noah-LSM uses meteorological forcing variables as input to simulate the land surface as a one-dimensional column. Previous research suggests that Noah-LSM, both in offline and

coupled mode, simulates climate variability and processes well in both semi-arid and mountainous regions (Hogue, 2003; Hogue et al. 2005; Jin and Miller, 2007). The work of this thesis is based on the offline 1-dimensional Noah-LSM version 3.4.1, which was released in September 2012 and is available at <http://www.ral.ucar.edu/research/land/technology/lsm.php>.

2.1.2 Noah-LSM Forcing Input and Simulation Output

The atmospheric and surface forcings required by Noah-LSM are fully described in Chen et al. (2007). Noah-LSM simulations require the input of eight meteorological forcing variables: (1) near-surface air temperature, (2) surface pressure, (3) near-surface wind speed, (4) near-surface wind direction, (5) near-surface relative humidity, (6) precipitation, (7) downward long wave radiation flux at the surface and (8) downward short wave radiation flux at the surface. Noah-LSM then simulates a number of state variables, including surface skin temperature, surface runoff, underground runoff, water-equivalent snow depth, snow depth, canopy moisture, ground heat flux, surface albedo, potential evaporation, and latent and sensible heat fluxes.

Though the offline, uncoupled Noah-LSM used in this work is a one-dimensional column model, it still considers the fractional coverage of vegetation, bare ground, land-use category, and soil category within each model grid cell. Noah-LSM has one canopy layer and uses a climatologically prescribed albedo and green vegetation fraction for each grid cell. Noah-LSM partitions the soil column into four soil layers with lower boundaries of 0.1m, 0.4m, 1.0m and 2.0m below the surface. From the surface to bottom soil layer, the soil layers in Noah-LSM represent the thin surface layer, root zone layer, deep root zone later and sub-root zone layer. For each soil layer, Noah-LSM simulates soil temperature, moisture content and liquid water content, allowing one to examine the diurnal and seasonal evolutions of the soil. A schematic of the model diagram is shown in Figure 2.



2.1.3 Noah-LSM Physics

The surface energy balance and surface water balance serve as the physically based foundation of Noah-LSM. Chen and Dudhia fully describe the model's hydrology and thermodynamics formulation (2001). Vertical water movement is governed by the conservation of water mass and a diffusive form of the Richard's equation for soil hydraulics (Richards 1931). The surface energy balance in Noah-LSM is used to compute the skin temperature of the ground-vegetation surface. Noah-LSM simulates temperature for each of the four soil layers using a Crank-Nicholson time-integration numerical scheme. Soil heat transfer in Noah-LSM is determined by diffusion equations. Additionally, Noah-LSM considers the relationships between soil moisture, hydraulic conductivity and soil matrix potential according to Clapp and Hornberger (1978). Noah-LSM uses a lookup parameter table based on a 24-category United States Geological Survey land-cover dataset to determine surface properties such as vegetation type, leaf area index, albedo and roughness length. Noah-LSM uses another lookup parameter table

based on a 16-category soil texture scheme that was developed by Miller and White to determine porosity, hydraulic properties, and the slope of the water retention curve (1998).

Moreover, we must consider the calculations of runoff and evapotranspiration in Noah-LSM, as diagnosing impacts to runoff and evapotranspiration is key to understanding the impacts of climate change on surface hydrology and water resources in the Los Angeles region. Noah-LSM simulates both surface and subsurface runoff. Surface runoff is parameterized in a simple infiltration-excess scheme, while subsurface runoff is treated as a linear function of bottom soil-layer gravitational drainage (Schaake et al. 1996). The lower 1m of the soil column acts as a reservoir with gravity drainage at the bottom, and the upper 1 m of soil serves as the root zone. Subsurface runoff in Noah-LSM is controlled by gravitational drainage alone. Surface runoff is then simply the excess water after infiltration occurs.

Total evapotranspiration in Noah-LSM has three contributing sources: direct evaporation from the top surface soil layer, evaporation of rainfall intercepted by the canopy, and transpiration via the canopy and roots. Transpiration via the canopy and roots is calculated according to the adjusted potential Penman-Monteith transpiration equation. The conductance of canopy transpiration is determined using the Jarvis scheme, where canopy resistance is calculated as a function of a number of environmental stress functions and the minimum canopy resistance (Jarvis 1976).

At high elevations in our study area, specifically in the San Gabriel, San Bernardino and San Jacinto Mountains, precipitation may fall as snow during the cold months of winter and early spring. Therefore, it is important to understand the treatment of snow in Noah-LSM. Using a single layer snow model, Noah simulates snowpack depth, snow water equivalent, snow albedo and skin temperature. Noah-LSM accounts for the accumulation, sublimation and heat exchanges at the snow-soil and snow-atmosphere boundaries. Unfortunately, Noah-LSM does not consider snow grain growth or changes over time. The presence of snow on the ground is essentially determined by air temperature, and Noah-LSM allows fractional snow cover within

grid cells (Ek et al. 2003). With the onset of snowmelt in the spring, melt water becomes runoff which does not affect the adjacent grid cells because Noah-LSM has no routing scheme.

2.2 Noah-LSM Initializations

This study focuses on two three-year time periods: A “baseline” period (September 1, 1998-August 31, 2001) and a “future” mid-21st century period (September 1, 2058 – August 31, 2061). By looking at differences between the future and baseline periods, mid-century changes to surface hydrology relative to the late 20th century can be evaluated in our study region. Additionally, the baseline simulation allows us to validate the model’s ability to simulate regional climate (section 3).

In order to have accurate initial conditions, a four-month spin-up technique was adopted for each of the six simulations. For the baseline simulation, Noah-LSM simulates near-surface states and fluxes over the Los Angeles region from May 1, 1998 to August 31, 2001; the future simulations run from May 1, 2058 to August 31, 2061. We treat the first four months of all simulations (May 1, 1998 to August 31, 1998 for the baseline simulation, and May 1, 2058 to August 31, 2058 for the future simulations) as the model spin-up period. Finally, we evaluate and analyze simulations of a three-year period: September 1, 1998 to August 31, 2001 for the baseline simulation and September 1, 2058 to August 31, 2061 for the future simulations. The Noah-LSM simulations are forced at a 3-hour time step by meteorological forcings simulated by WRF. A detailed description of the methods used to produce the meteorological forcing inputs for the Noah-LSM simulations is found in section 2.3.

We run six offline Noah-LSM simulations in this study: (1) a baseline simulation forced by WRF dynamically-downscaled NARR; (2) a future simulation forced by WRF dynamically-downscaled NARR perturbed by CCSM4; (3) a future simulation forced by WRF dynamically-downscaled NARR perturbed by CNRM-CM5; (4) a future simulation forced by WRF dynamically-downscaled NARR perturbed by GFDL-CM3; (5) a future simulation forced by WRF

dynamically-downscaled NARR perturbed by MIROC-ESM-CHEM; and (6) a future simulation forced by WRF dynamically-downscaled NARR perturbed by MPI-ESM-LR. All future simulations use RCP8.5 to determine the climate change signal that is generated by the WRF model and used to force Noah-LSM.

2.3 Meteorological Forcing Inputs for Noah-LSM Simulations

Using dynamical downscaling techniques and the Weather Research and Forecasting (WRF) Model, we project meteorological forcing variables for the Los Angeles region at 2km resolution for the baseline period and future period under Representative Concentration Pathway 8.5 as projected by five global climate models in the CMIP5 data archive. A more complete description of the WRF technique to simulate meteorological forcing inputs for the Noah-LSM simulations is found in Hall et al. (2012).

2.3.1 Global climate simulations

General circulation models (or global climate models, GCMs) simulate global atmospheric and meteorological variables for a large area (resolution ranging from 2.5° – 10° longitude and latitude); they are widely used for projecting global climate change that results from increasing concentrations of greenhouse gases in the atmosphere. Variables simulated in GCMs include radiative fluxes, sea level pressure, specific humidity, precipitation, temperature and wind velocities. We use a data archive of multi-model global climate change experiments, the Coupled Model Intercomparison Project Phase 5 (CMIP5) (Taylor et al. 2012). CMIP5 contains simulated output from nearly 30 state-of-the-art GCMs from various climate research centers. The CMIP5 archive was designed to advance the scientific community's knowledge of climate variability and climate change. CMIP5 forms the bases of the forthcoming Fifth Assessment Report (AR5) by the United Nations Intergovernmental Panel on Climate Change (IPCC).

By coordinating simulations from numerous GCMs, multi-model ensemble simulations

can be evaluated. Previous research has shown that multimodel ensemble simulations outperform individual model simulations and provide more robust estimates of future climate change and uncertainties (Gleckler et al. 2008, Sillman et al. 2013). CMIP5 utilizes emission scenarios called Representative Concentration Pathways (RCPs) (Moss et al. 2010, Meinhausen et al. 2011). While four RCPs have been assessed, the work of our study focuses on RCP 8.5, which corresponds to a produced radiative forcing of 8.5 watts per square meter by the end of the 21st century due to increasing greenhouse gas concentrations. The RCP8.5 scenario would be one in which greenhouse gas emissions continue to increase throughout the 21st century. We choose RCP8.5 because of its strong signal at the end of the 21st century. RCP8.5 is very similar to the A2 emissions scenario of the Special Report on Emissions Scenarios (SRES), which was used for the CMIP3 model comparison project (Moss et al. 2010).

While GCMs are valuable in assessing general trends over regions, their coarse resolution fails to capture atmospheric and meteorological variables at a resolution necessary for performing regional-scale analysis (Giorgi and Mearns, 1991). The average resolution of CMIP5 models is about 200km, which is far too low to understand surface hydrology and climate at scales relevant to policy makers or water resources planners. Los Angeles' topographical features and coastlines are poorly represented in GCMs, and thus GCMs cannot simulate regional-scale processes (including the coastal vs. desert climates in the Los Angeles Region, land-sea breeze circulations, valley climates and orographic precipitation). These phenomena are important in understanding and projecting the surface hydrology of the Los Angeles region. Previous research also suggests that the consideration of regional-scale processes is necessary in order to understand and simulate climate variability and hydrology in California (Cayan, 1996; Conil and Hall, 2006; Hughes et al. 2007). The scale of GCMs is simply too coarse to accurately force high-resolution Noah-LSM runs for our study domain.

Therefore, in order to obtain reliable surface hydrology information for Los Angeles at the regional-scale from Noah-LSM, we must force Noah-LSM with meteorological variables

downscaled from the relatively-course GCMs to a spatial scale of much higher resolution. In the case of our Noah-LSM simulations, we need atmospheric and meteorological variables at 2km resolution to force our model. Though GCMs are unable to provide such high-resolution forcings, downscaling methods have been developed in order to simulate detailed climatology for smaller regions.

2.3.2 WRF and dynamical downscaling methods to produce Noah-LSM forcing inputs

Translating coarse-resolution GCM simulations to the local or regional scale is challenging. Both dynamical and statistical downscaling methods have been used to develop detailed high-resolution climatology from GCM simulations. In our case, we employ dynamical downscaling to simulate high-resolution meteorological variables from the relatively coarse-resolution GCM output. The high-resolution meteorological variables of temperature, surface pressure, wind speed, wind direction, relative humidity, precipitation, incoming long wave radiation and incoming shortwave radiation are then used to force our Noah-LSM simulations.

Dynamical downscaling involves the use of mesoscale atmospheric models, which describe the domain topography and land surface at a much higher spatial resolution than GCMs. In dynamical downscaling, regional climate models are nested within a coarse-resolution GCM grid cell with either GCM simulation output or reanalysis data as the lateral boundary conditions for the simulation. Then, atmospheric dynamics are modeled at a very high resolution, allowing the regional climate model to simulate fine-scale physical processes. Dynamical downscaling greatly decreases the model's spatial resolution (1km to 50km) and has been widely used to explore climate change impacts over a variety of regions (Jones et al. 1997; Giorgi et al. 2001; Wang et al. 2004). Dynamical downscaling has already proven valuable in obtaining high-resolution information on California climate change from coarse-resolution GCM simulations (Leung et al. 2003; Leung et al. 2004; Kanamitsu and Kanamaru,

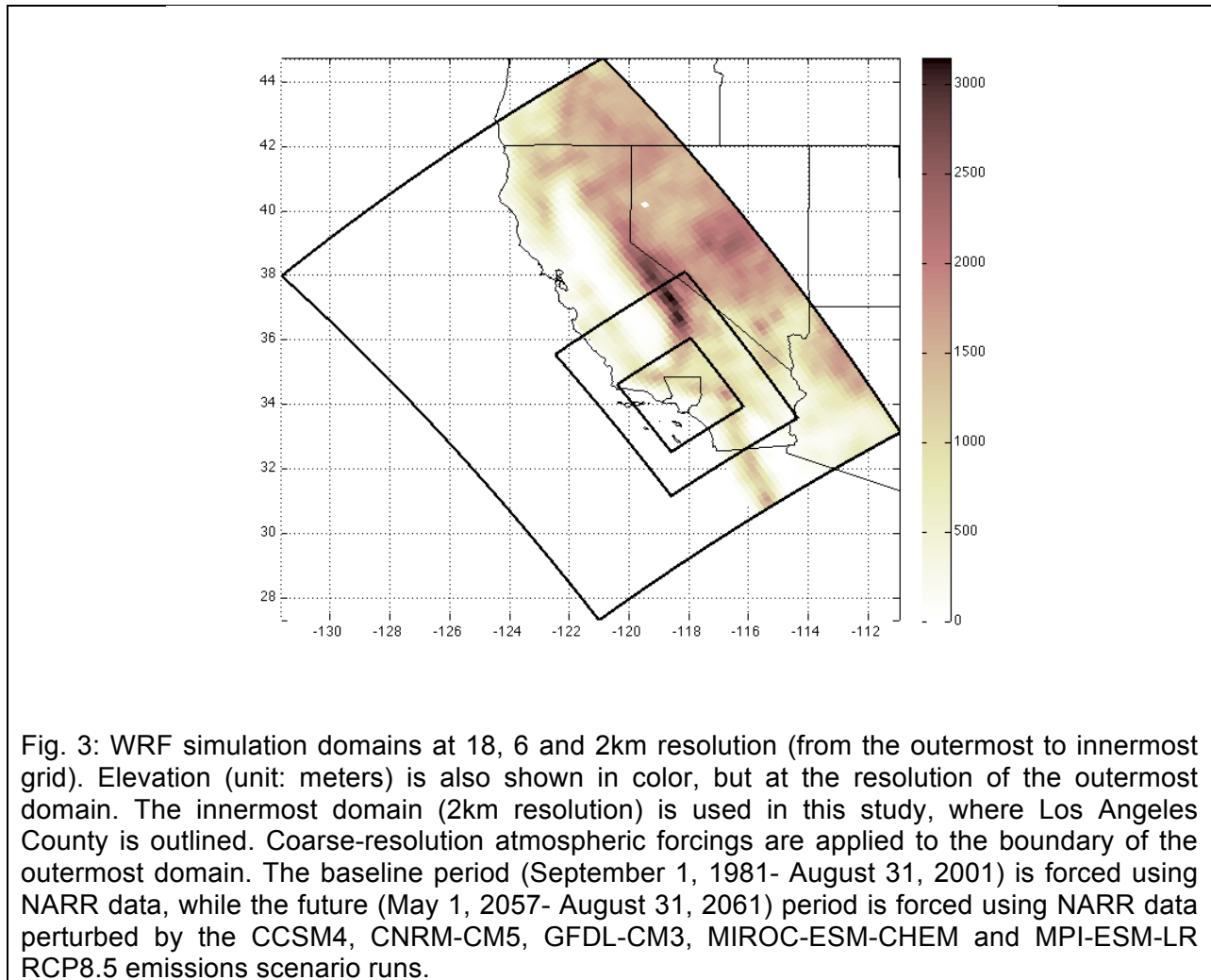
2007; Caldwell et al. 2009; Qian et al. 2010; Pan et al. 2011). Previous research has assessed impacts to California's temperature, snowpack and hydrologic cycle. Unfortunately, dynamical downscaling techniques require extensive computing power, making it highly impractical to dynamically downscale every GCM in the CMIP5 data archive forced by each emissions scenario. Thus, we choose to dynamically downscale five GCMS in the CMIP5 data archive for emissions scenario RCP8.5

To dynamically downscale GCM output and reanalysis data to a finer resolution in the Los Angeles region, we use the Weather Research and Forecasting Model (WRF; Skamarock et al. 2008) version 3.2. WRF is a mesoscale forecast model developed by the National Center for Atmospheric Research (NCAR). WRF is designed for simulations at the regional scale and is well suited for a wide range of applications, including idealized climate simulations and operational weather forecasts. Some key features of WRF include: (1) fully compressible Euler non-hydrostatic equations; (2) high-order numerical techniques that conserve mass and dry entropy; (3) scalar-conserving flux form for prognostic variables; and (4) nesting capability.

As a community-developed model, WRF offers numerous physics parameterization options, thus tapping into the knowledge and experience of the modeling community. The physics parameterization options allow the model to be applicable on scales ranging from tens of meters to thousands of kilometers. We choose the following physics parameterization options for our simulations: Kain-Fritsch cumulus scheme (Kain, 2004); Yonsei University boundary layer scheme (Hong et al. 2006); Purdue Lin microphysics scheme (Lin et al. 1983); Rapid Radiative Transfer Model longwave radiation (Mlawer et al. 1997); and Dudhia shortwave radiation schemes (Dudhia, 1989).

Figure 3 shows the domains for the WRF simulations. To increasingly link the scales of the coarse resolution GCMs output to a high-resolution simulation of the Los Angeles region, we successively nest higher resolution domains within one another. Each outer domain then feeds the lateral boundary conditions to a higher-resolution domain nested within it. In our WRF

simulations, there are three nested domains. The outermost domain, with the coarsest horizontal resolution of 18km, simulates the state of California along with the adjacent Pacific Ocean. The second domain focuses on the southern portion of California with a resolution on 6km. Finally, the innermost domain, with the highest resolution of 2km, examines the Los Angeles region and surrounding areas.



To ensure a smooth transition across the boundary from one nested domain to another nested domain, we relax grid points near the lateral boundaries to the corresponding values at the boundaries separating the domains. Each nested domain has 43 sigma-levels in the vertical, and the vertical resolution is enhanced near the surface as 30-sigma levels are within 3km of the surface. Finally, the innermost domain in the dynamical-downscaling WRF runs is the same

domain as the Noah-LSM simulations described in the previous section (seen in figure 1).

Using this WRF model configuration, we perform a twenty-year baseline simulation (September 1, 1981- August 31, 2001) to reconstruct weather and climate variations at 2km resolution. The output from May 1, 1998 to August 31, 2001 serves as the meteorological forcing input for the baseline Noah-LSM simulation previously described (where the first four months are considered the spin-up period for the Noah-LSM simulations). We choose to analyze the three years from September 1, 1998 to August 31, 2001 for the Noah-LSM simulations, as they represent rather average years of the baseline period in terms of annual mean temperature. This period also samples the interannual variability of temperature and precipitation in our domain well. The coarse-resolution (32km) data archive used to force the WRF regional model for the baseline simulation is the National Centers for Environmental Prediction 3-hourly North America Regional Reanalysis (NARR) data. NARR data serves as the lateral boundary conditions for the outermost domain in figure 3 for the baseline simulation.

Table 1: Name and characteristics (country, institution, and resolution) of the CMIP5 GCMs used for WRF dynamical downscaling.

Model Name	Country	Institute	Resolution
CCSM4	USA	National Center for Atmospheric Research	1.25° x .9°
CNRM-CM5	France	Centre National de Recherches Meteorologiques	1.4° x 1.4°
GFDL-CM3	USA	NOAA Geophysical Fluid Dynamics Laboratory	2.5° x 2.0°
MIROC-ESM-CHEM	Japan	AORI (U. Tokyo), NIES, JAMSTEC	2.8° x 2.8°
MPI-ESM-LR	Germany	Max Planck Institute for Meteorology	

As mentioned earlier, dynamical downscaling techniques are very computationally expensive, and that is why we can only dynamically downscale five GCMs in the CMIP5 data archive for emissions scenario RCP8.5 for short simulations. It would be highly impractical and expensive to dynamically downscale every GCM for multiple emissions scenarios and long

durations, though that would certainly help in characterizing climate change uncertainties. The five GCMs we select from the CMIP5 archive are chosen as they simulate a range of different regional-mean warming signals and land-sea warming contrasts in our domain.

To produce future boundary conditions for WRF, we quantify the differences in monthly climatology between the future and baseline periods for each GCM; these differences represent the climate change signals of interest that develop in each GCM simulation. For each month and each GCM, the climate change signals are added to the NARR reanalysis data corresponding to the baseline period. Additionally, we increased carbon dioxide levels in the future WRF simulations to match the change in carbon dioxide equivalent radiative forcing in the RCP8.5 emissions scenario. As a result, we perturb the NARR data with the climate change signal provided by the five GCMs to have five sets of boundary conditions for the future: (1) NARR perturbed by CCSM4; (2) NARR perturbed by CNRM-CM5; (3) NARR perturbed by GFDL-CM3; (4) NARR perturbed by MIROC-ESM-CHEM; and (5) NARR perturbed MPI-ESM-LR.

For both the baseline (1998-2001) and five future (2058-2061) dynamically downscaling climate simulations, WRF output includes snapshots of 2-dimensional variables every 3 hours and 3-dimensional variables every 6 hours for each gridpoint. The 3-dimensional variables were interpolated from a 6-hour time step to a 3-hour time step for all Noah-LSM simulations.

3 Validation

Prior to analyzing changes to surface hydrology in the Los Angeles region, we demonstrate that the offline Noah-LSM baseline simulation accurately simulates the mean state. Since the focus of this study is the surface hydrological component of climate change, the validation exercise involves a comparison of simulated variations by the offline Noah-LSM runs and observed variations related to surface hydrology. A second component of the validation exercise involves the validation of the meteorological variables from the dynamical downscaling WRF simulations used to force the Noah-LSM simulations.

Noah-LSM model performance for the baseline period is evaluated by comparing simulated model output of soil temperature, evapotranspiration and surface runoff to available point measurements. Unfortunately, other variables are unable to be validated due to limited observational measurements in our study domain. In this section, we describe the data available for evaluation as well as the model's ability to reproduce climate variations within the Los Angeles region. In our comparison between model output and point-measurements, we focus on the period between September 1, 1998 and August 31, 2001 (the validation period).

3.1 Evaluation data

3.1.1 CIMIS Observation Stations

The California Irrigation Management Information System (CIMIS) consists of a network of over 130 computerized weather stations throughout the state of California (Hart et al. 2008). The California Department of Water Resources and the University of California, Davis implemented CIMIS stations in 1982. CIMIS stations are located near key municipal and agricultural sites, as the original intention of the stations was to provide evapotranspiration data to the agricultural community in order to improve water use. Stations collect hourly data of air temperature, wind speed, wind direction, soil temperature, solar radiation, evapotranspiration and relative humidity. We obtained hourly, quality-controlled, near-surface meteorological

observations from 17 CIMIS stations (CIMIS #10, 11, 58, 59, 73, 75, 78, 82, 93, 97, 99, 101, 102, 117, 125, 133 and 159) within our study domain for which data was available for the validation period at <http://www.cimis.water.ca.gov/cimis/>. The length and completeness of the observational record, as well as the measured meteorological variables, vary for each CIMIS station. The network of CIMIS stations used for model evaluation is shown in figure 4.

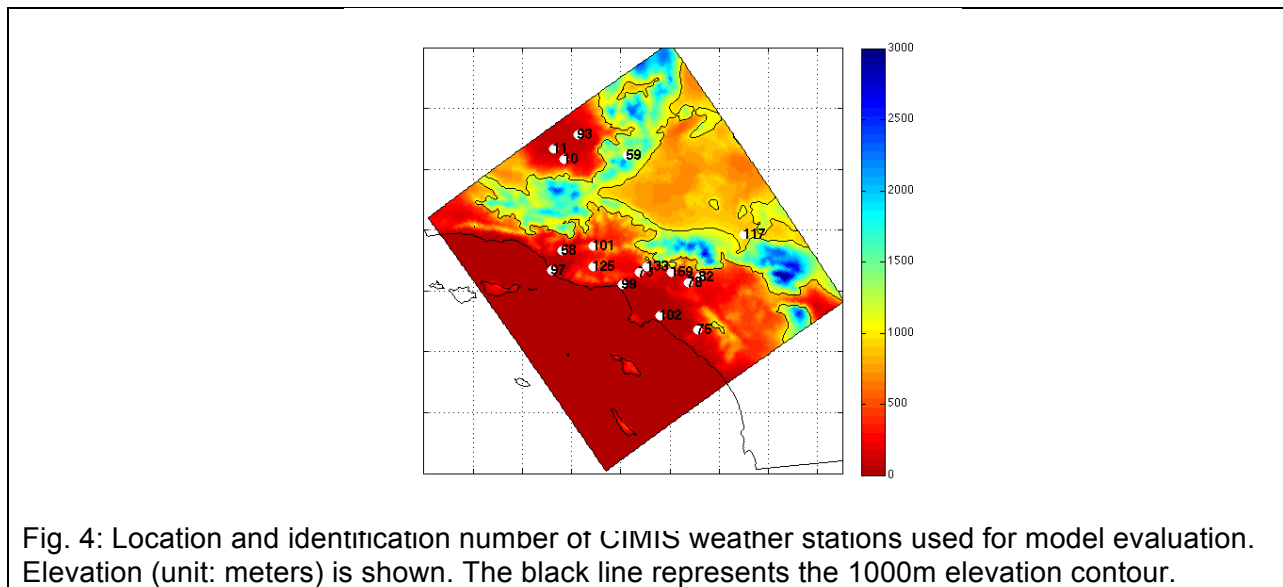
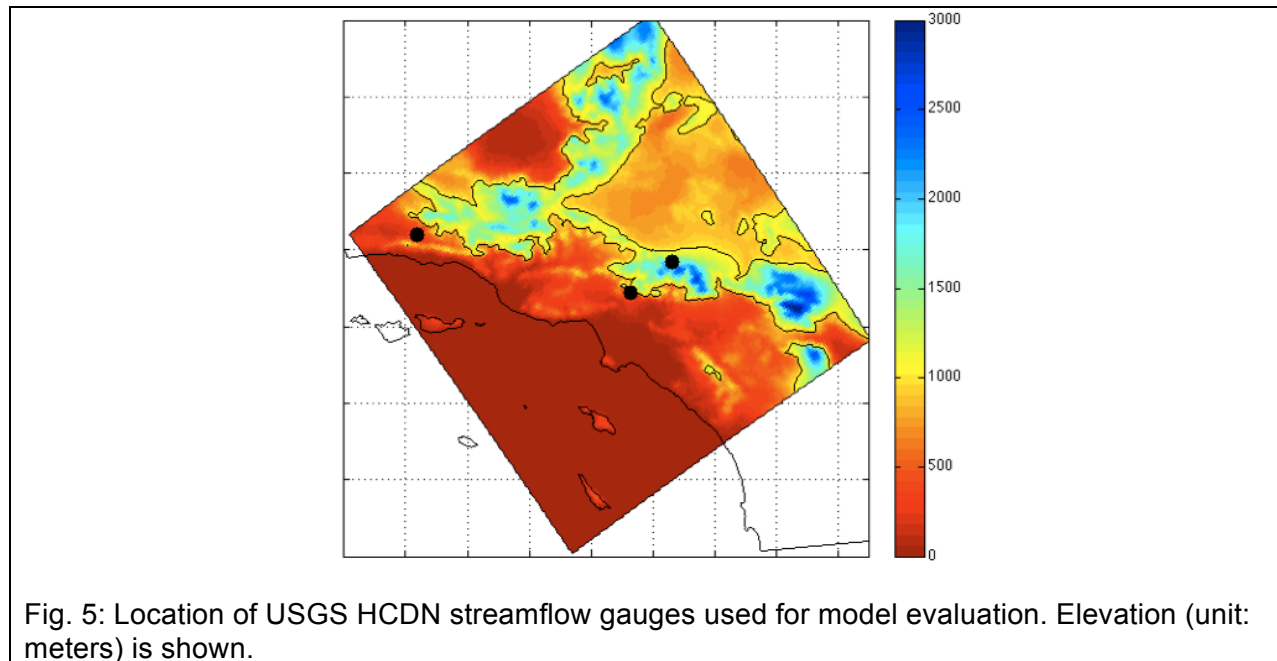


Fig. 4: Location and identification number of CIMIS weather stations used for model evaluation. Elevation (unit: meters) is shown. The black line represents the 1000m elevation contour.

3.1.2 USGS HCDN Streamflow Gauges

Noah-LSM model performance for the baseline period is also evaluated by comparing simulated output of surface runoff to available point measurements from streamflow gauges from the United States Geological Survey (USGS) Hydro-Climatic Data Network-2009 (HCDN-2009). The USGS HCDN-2009 is a network of streamflow gauges across the United States (Slack et al. 1993; Lins, 2012). Streamflow data is available through the National Water Information System of the USGS at <http://waterdata.usgs.gov/nwis/>. HCDN-2009 streamflow gauges are identified as having natural streamflows least affected by direct human activities, accurate measurement records, and at least 20 years of complete and continuous discharge record through water year 2009. We obtained daily, quality-controlled streamflow data from 3 gauging stations (USGS gauges 10263500, 11098000 and 11124500) for which data was

available within our study domain for the validation period. All gauges have complete records of daily streamflow discharge data for validation period. The network of HCDN streamflow gauges used for model evaluation is shown in figure 5.



3.2 Validation of Noah-LSM Output

We validate Noah-LSM model performance for the baseline period by comparing simulated output of soil temperature, evapotranspiration and runoff to observational point measurements from the CIMIS weather stations and USGS HCDN-2009 streamflow gauges. The networks of available point measurements seen in figures 4 and 5 are far too sparse to adequately characterize all spatial and temporal patterns output by Noah-LSM. However, because the locations of observational measurements represent a variety of elevations, vegetation types, soil types and distances from the coast, we can use the networks of available point measurements to evaluate the realism of the spatial and temporal patterns simulated by Noah-LSM. The variety of locations provides a nice sampling of the range of soil temperatures, evapotranspiration rates and runoff observed across our domain. This section will discuss validation methods for the Noah-LSM output. Additionally, we demonstrate that Noah-LSM

properly simulates the observed spatial patterns and mean state of surface hydrology in our domain.

3.2.1 Soil temperature

We validate daily minimum and maximum soil temperature, which is output by Noah-LSM. Thirteen CIMIS stations have some record of hourly soil temperature at 15cm depth during the validation period. Noah-LSM outputs soil temperature for each of the four soil layers. Soil temperatures the thin surface layer and root zone layer are representative of the mean temperature between 0-10cm and 10-40cm, respectively. As such, we take a weighted mean of the simulated soil temperature of layers 1 and 2 in order to determine the temperature at 15cm depth. Figure 6 (7) compares the seasonal-mean daily minimum (maximum) temperature observed at a CIMIS point measurement site to the seasonal-mean daily minimum (maximum) temperature simulated at the nearest grid point in the WRF domain for thirteen CIMIS point measurement sites. This comparison provides an assessment of the realism of the spatial and seasonal patterns simulated by Noah-LSM.

The seasonal cycle of daily minimum and maximum soil temperatures simulated by Noah-LSM is very much consistent with observations. The seasonal shifts in daily maximum and minimum soil temperature at 15cm depth are almost identical at the CIMIS observational locations and the nearest model grid points. This confirms that for each season, the model simulates the spatial variations in climatological daily maximum and minimum soil temperature at 15cm depth quite well. The model quality is particularly good in fall, winter and spring, with correlations above .75 for both maximum and minimum daily temperature. WRF tends to underestimate the maximum and minimum daily soil temperatures at 15cm depth during the summer, but the model and observations are still in broad agreement during this season. Overall, figures 6 and 7 give us confidence in the model's ability to simulate accurate states.

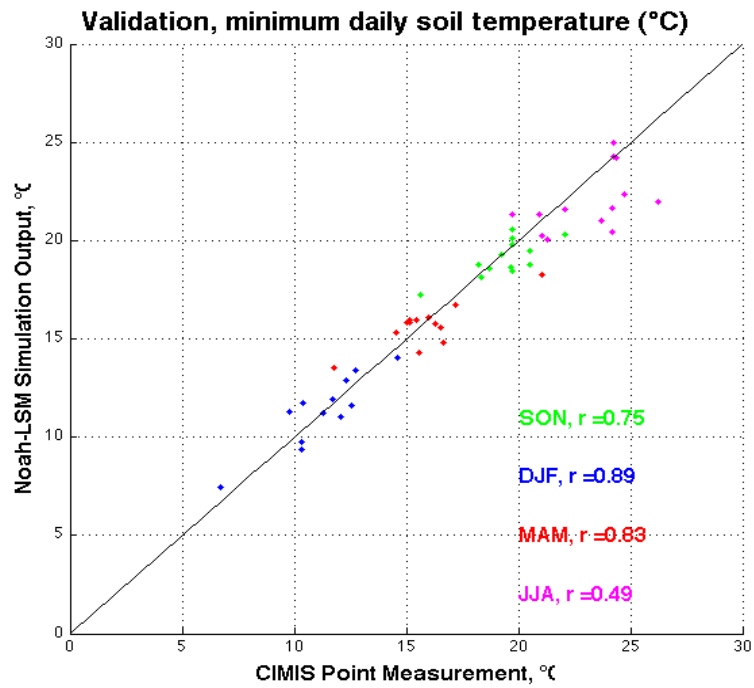


Fig. 6: Validation of the spatial variability of minimum daily soil temperature as simulated by Noah-LSM. This shows a comparison of the average seasonal-mean minimum daily soil temperature ($^{\circ}\text{C}$) at a CIMIS point measurement site to the seasonal-mean minimum daily soil temperature simulated at the nearest grid point in Noah-LSM for thirteen point measurement sites. Points are color-coded by season. Observed daily minimum soil temperatures are highly correlated with simulated daily minimum soil temperatures in each season.

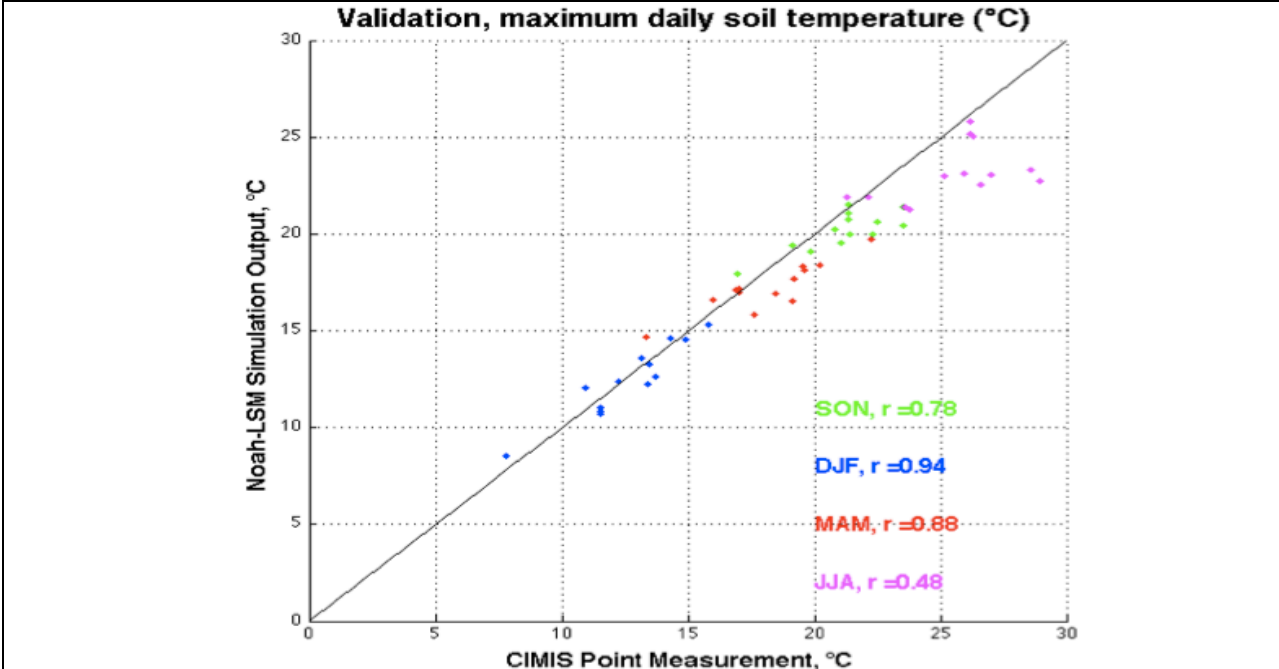


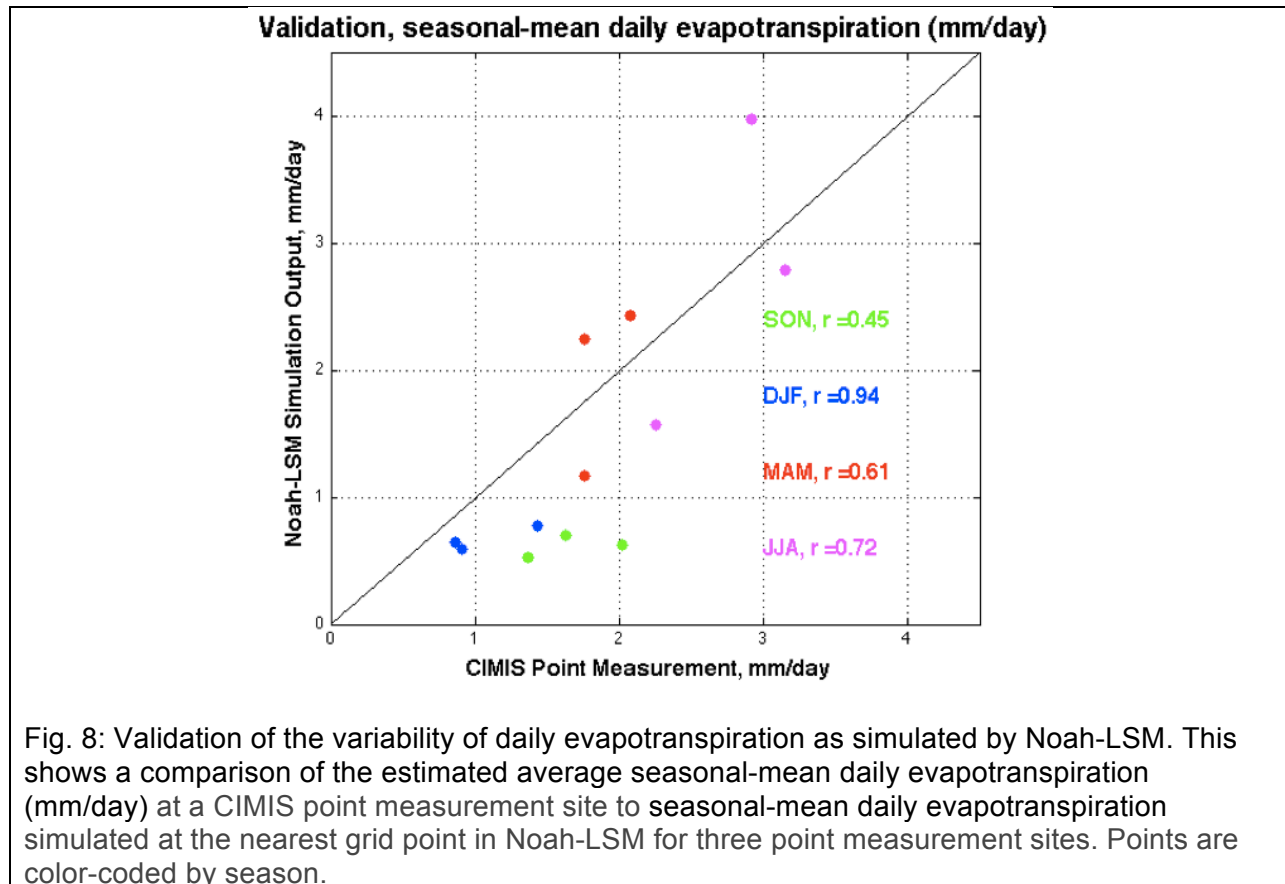
Fig. 7: Validation of the spatial variability of maximum daily soil temperature as simulated by Noah-LSM. This shows a comparison of the average seasonal-mean maximum daily soil temperature (°C) at a CIMIS point measurement site to the seasonal-mean maximum daily soil temperature simulated at the nearest grid point in Noah-LSM for thirteen point measurement sites. Points are color-coded by season. Observed daily maximum soil temperatures are highly correlated with simulated daily maximum soil temperatures in each season.

3.2.2 Evapotranspiration

We validate evapotranspiration, which is output by Noah-LSM and estimated by CIMIS stations. CIMIS provides evapotranspiration estimates at specific sites, and three CIMIS weather stations in our domain have adequate meteorological data to estimate daily evapotranspiration for our the validation period; other CIMIS stations do not have adequate measurements to estimate daily evapotranspiration. Evapotranspiration has high spatial variability due to the complex interactions between topographical features and the nature of climate itself. Evapotranspiration is influenced by a number of factors, including solar radiation (which is itself highly affected by cloud cover), air temperature, relative humidity and wind speed. Additionally, soil factors (including soil texture and density) and plant factors (including plant type and root depth) influence evapotranspiration. Direct measurement of daily evapotranspiration rates is both expensive and time consuming, and thus evapotranspiration

estimates through both analytical and empirical equations is common. CIMIS employs the standardized Penman-Monteith equation for estimating reference evapotranspiration as described by Allen et al. (1998, 2006)

Figure 8 compares climatological evapotranspiration for CIMIS locations and the nearest model grid point, providing an assessment of the surface hydrology climatology simulated by Noah-LSM. The seasonal cycle of daily evapotranspiration simulated by Noah-LSM is broadly consistent with observations. Daily evapotranspiration is greatest during the summer months when more energy is available for evapotranspiration (due to higher incoming solar radiation during the summer) and both the vegetative cover and leaf area index are highest. In the winter, though surface water availability is high at high elevations in our domain, evapotranspiration is lowest due to limited energy availability and a lower leaf area index. Thus, Noah-LSM accurately simulates the seasonal shifts in daily evapotranspiration.

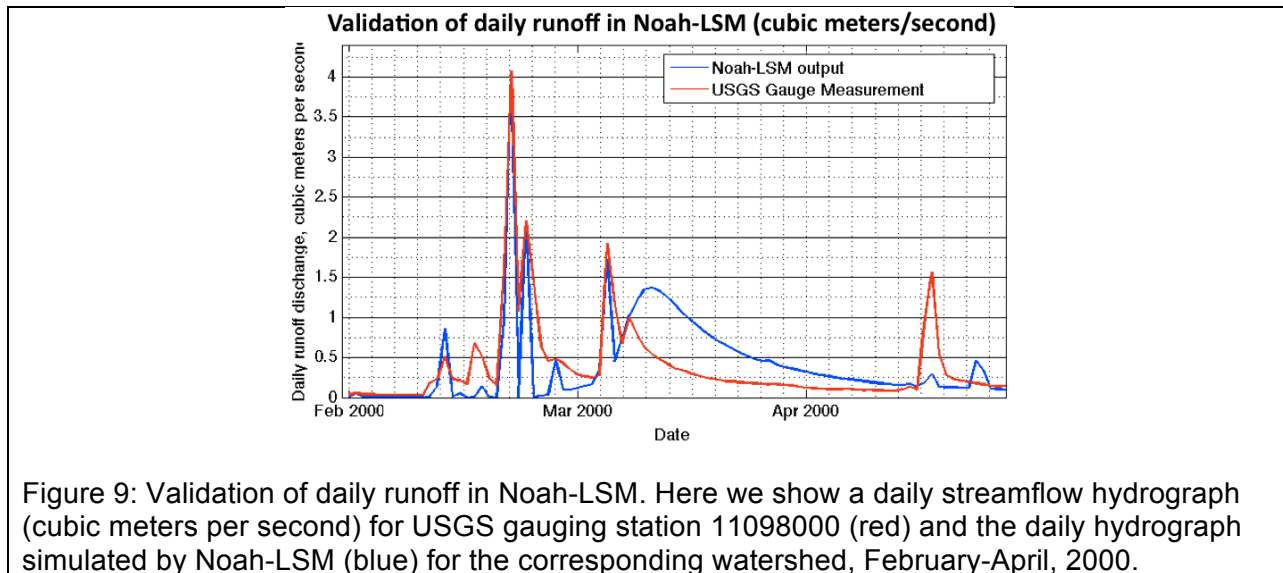


While Noah-LSM successfully captures the seasonal cycle of daily evapotranspiration, the model appears to have trouble capturing the exact magnitude of daily evapotranspiration with high accuracy. Within each season, evapotranspiration as simulated by Noah-LSM is often an underestimation or overestimation of the observed CIMIS measurement. However, there seems to be neither a strong bias toward evapotranspiration overestimation nor toward evapotranspiration underestimation and evapotranspiration as simulated by Noah-LSM is usually within 1-2 mm/day of the CIMIS estimate. It is difficult to compare CIMIS observations for evapotranspiration to the nearest model gridpoint because of the highly variable nature of spatial evapotranspiration patterns. Even with a fine model resolution of 2km, the nearest Noah-LSM gridpoint to a CIMIS observation station can be as far as 1.4km. Evapotranspiration varies within very fine spatial scales due to differences in vegetative cover, soil type, land use category, etc. The spatial gap and difference in surface characteristics between CIMIS stations and Noah-LSM grid points could account for the underestimation of evapotranspiration during the fall and winter. We also compared the CIMIS estimate of daily evapotranspiration to the mean of the closest two, three or four Noah-LSM grid points, but the validation does not improve. As a result, we are confident in Noah-LSM's ability to simulate the seasonal cycle of daily evapotranspiration as well as realistic evapotranspiration values.

3.2.3 Runoff

We also validate Noah-LSM model performance for the baseline period by comparing simulated output of surface runoff within a watershed to the observed value from the USGS streamflow gauging station in the corresponding watershed. Three USGS streamflow gauging stations are used to evaluate model performance. Noah-LSM has no routing scheme, and runoff is simply removed from the model immediately. Therefore, to compare streamflow discharge measured at a gauging station to Noah-LSM output, we take the sum of the runoff for each gridpoint in the watershed that drains to the USGS gauging station in our domain.

A comparison between the daily runoff measured at USGS streamflow gauge 11098000 and the runoff simulated in Noah-LSM for the corresponding watershed is shown in figure 9 for February-April, 2000. Noah-LSM accurately captures the temporal variability of runoff as measured at the streamflow gauge. Moreover, Noah-LSM the average monthly magnitude of discharge is well represented by Noah-LSM. Average flow for this hydrograph as simulated by Noah-LSM is .39 cubic meters per second, while the average flow for this hydrograph as measured at gauge 11098000 is .38 cubic meters per second. Realistically simulating runoff magnitude is important from a water-resources perspective. Often, Noah-LSM runoff output is either too responsive or not responsive enough to small inputs of precipitation; peak runoff rates as simulated in Noah-LSM are often too high, while persistent low flows are often too low. Moreover, after precipitation events, Noah-LSM has trouble capturing the speed at which runoff flow recedes.



For the three gauging stations over the course of the entire validation period, the daily runoff rates simulated by Noah-LSM are highly correlated (>.87) with the measured rates at the streamflow gauging station. Moreover, the seasonal cycle of daily runoff as simulated by a watershed in Noah-LSM is very much consistent with the seasonal cycle of daily streamflow at the gauging station in that watershed. This confirms that for each season, the model simulates

the spatial variations in daily runoff quite well. Overall, the ability of Noah-LSM to simulate runoff in our domain and figure 9 give us confidence in the model's ability to simulate accurate surface hydrology.

3.3 Validation of dynamically downscaled WRF output used to force Noah-LSM simulations

We evaluate the dynamically downscaled WRF output that is used to force the offline Noah-LSM simulations by comparing the simulated output to available point measurements and gridded observation products. In this section, we discuss previous validation of the WRF temperature and precipitation output. Additionally, we validate the WRF output of average seasonal-mean incoming solar radiation and average seasonal-mean relative humidity, as both meteorological variables are used to force the Noah-LSM simulations.

Previous studies have already evaluated the temperature and precipitation output from the WRF simulations described in this paper. Hall et al. validates the WRF simulation's ability to capture both the spatial and temporal variability of temperature in the Los Angeles region for the baseline simulation (2012). They observed a high correlation between observed temperatures and WRF simulated temperatures in each season when comparing the average seasonal-mean temperature observed at a point measurement site to the seasonal temperature simulated at the nearest grid point in the WRF domain for 24 point measurement sites. The point measurement sites are near-surface temperature observations from 24 weather stations obtained from the National Climatic Data Center (NCDC; <http://www.ncdc.noaa.gov/oa/ncdc/html>). Additionally, they found the WRF framework realistically simulates the intermonthly and interannual variability in temperature for these simulations.

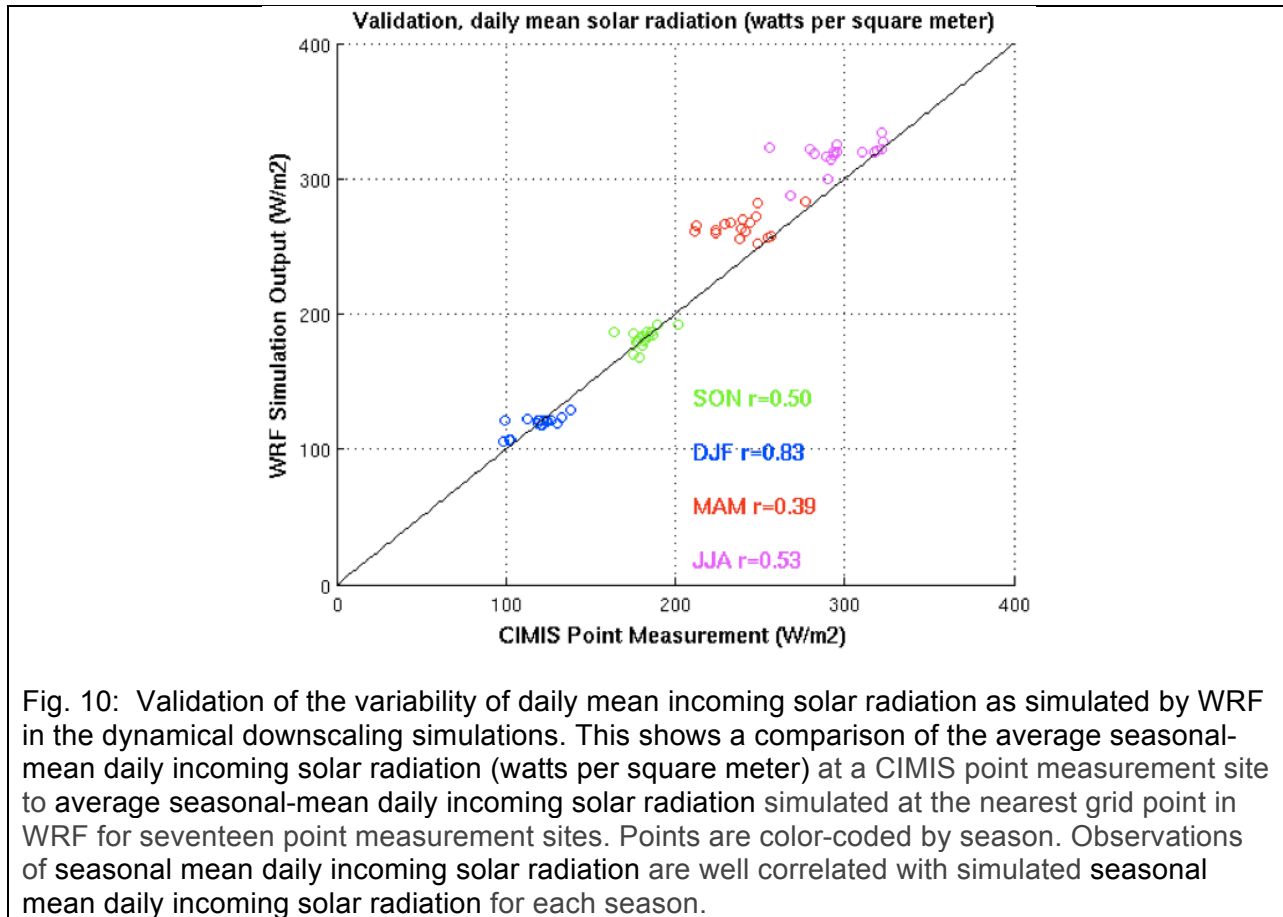
Ongoing research by Berg et al. (2013) demonstrates that the WRF framework realistically simulates both spatial and temporal patterns of wet-season (December-March)

precipitation in our domain. Using CIMIS gauges and two gridded observations products, CPC (<http://www.esrl.noaa.gov/psd/data/gridded/data.unified.html>) and Udel (http://www.esrl.noaa.gov/psd/data/gridded/data.UDel_AirT_Precip.html), they find high correlations between observed wet-season precipitation values and the simulated wet-season precipitation at the nearest grid point in the WRF domain. Moreover, they find that the WRF framework realistically simulates the interannual variability in wet-season precipitation for these simulations.

In addition to prior research's validation of precipitation and near surface temperature, we validate daily mean solar radiation, which is output by the WRF simulations and used as a forcing variable for the offline Noah-LSM simulations. Figure 10 compares the average seasonal-mean incoming solar radiation observed at a CIMIS point measurement site to the seasonal incoming solar radiation simulated at the nearest grid point in the WRF domain for seventeen point measurement sites. This comparison provides an assessment of the realism of the spatial and seasonal patterns of the meteorological forcing variables for the offline Noah-LSM simulations. The seasonal cycle of incoming solar radiation simulated by the model is highly consistent with observations. The seasonal shifts in incoming solar radiation are nearly identical at the observational locations and the nearest model grid points. In addition, within each season, the observed climatological incoming solar radiation is well correlated with its simulated counterpart across our simulation domain. This confirms that for each season, the model simulates the spatial variations in climatological incoming solar radiation reasonably well.

The model quality is particularly high in winter (.83). During spring and summer, the model and observations are still in broad agreement, though the correlation is somewhat lower as the models tend to overestimate incoming solar radiation. This could perhaps be due to the WRF's inability to capture May Gray and June Gloom, a localized phenomenon whereby low marine stratocumulus clouds are common over Southern California in May and June (Klein and Hartmann, 1993). Overall, figure AD, along with previous and ongoing research, gives us

confidence that the dynamical-downscaling WRF simulations give the right spatial and temporal variations in incoming solar radiation, near-surface temperature and precipitation in our domain. This leads us to believe that the offline-Noah simulations are forced with realistic input. Moreover, the validation of these variables gives us confidence that WRF provides a realistic downscaling of the regional pattern in the coarser resolution NARR data set.



3.4 Water budget closure

We also validate output from the offline Noah-LSM simulations by ensuring the baseline output satisfies the surface water balance equation. The balance of surface water requires that water sources to the surface equal water sinks from the surface. Therefore, precipitation must equal the sums of runoff, evapotranspiration and the change in soil water storage. One cannot analyze changes to surface hydrology without a closed water budget.

In a semi-arid region like Los Angeles, the soil is rather dry (see figure 18) and any changes to the soil water storage term are even smaller. Thus, the soil water storage term is nearly negligible for this domain and precipitation should roughly equal the sum of runoff and evaporation at each grid point. Because there is no routing scheme in Noah-LSM, we do not need to consider the transfer of surface water between adjacent grid cells.

Figure 11 demonstrates that Noah-LSM output for the baseline simulation precisely satisfies the surface water balance equation for nearly all grid points. There is a very high correlation (.96) between annual precipitation and the sum of annual evapotranspiration and annual runoff, showing that Noah-LSM properly simulates a closed water budget for the baseline period.

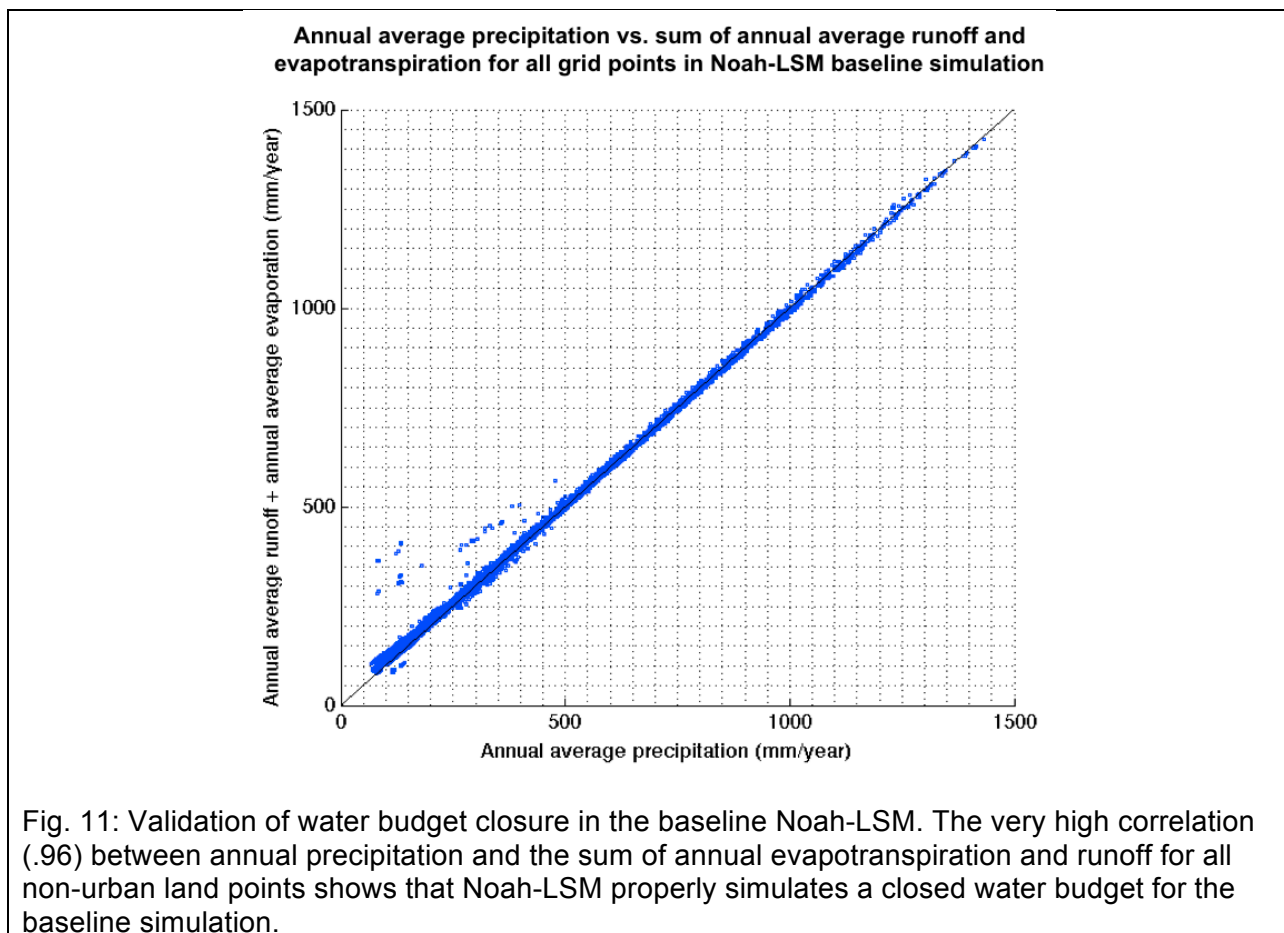
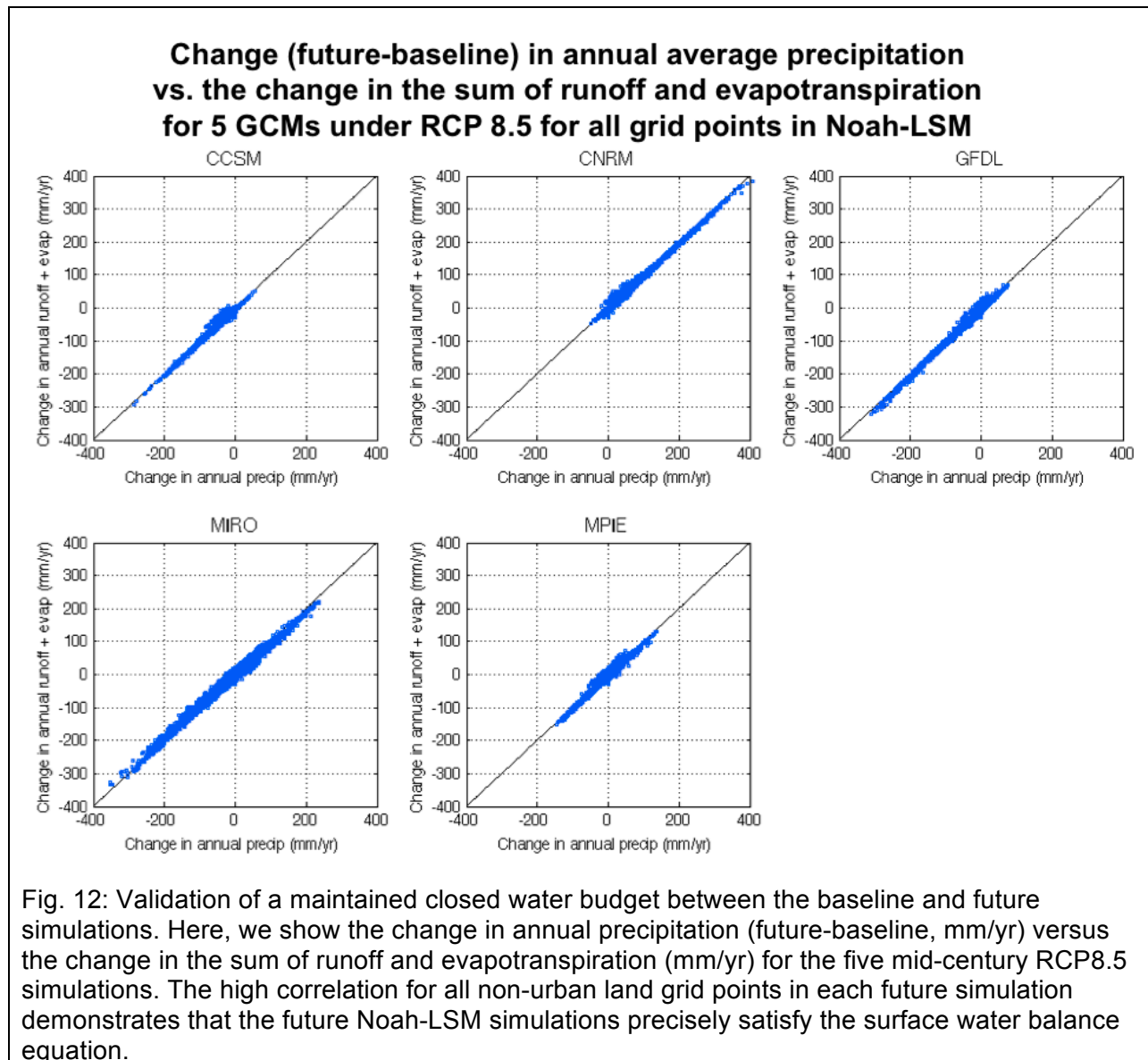


Fig. 11: Validation of water budget closure in the baseline Noah-LSM. The very high correlation (.96) between annual precipitation and the sum of annual evapotranspiration and runoff for all non-urban land points shows that Noah-LSM properly simulates a closed water budget for the baseline simulation.

Figure 12 shows the change in annual precipitation (future-baseline) versus the change in the sum of runoff and evapotranspiration for the five mid 21st century RCP8.5 simulations. This figure demonstrates that Noah-LSM output for the five future simulations precisely satisfies the surface water balance equation, as there is a high correlation (>.97) between the change in annual precipitation and the sum of the changes in annual runoff and annual evapotranspiration for all grid points in each future simulation. Overall, figures 11 and 12 give us confidence that Noah-LSM accurately simulates a closed water budget, which allows us to analyze changes to surface hydrology states and fluxes.

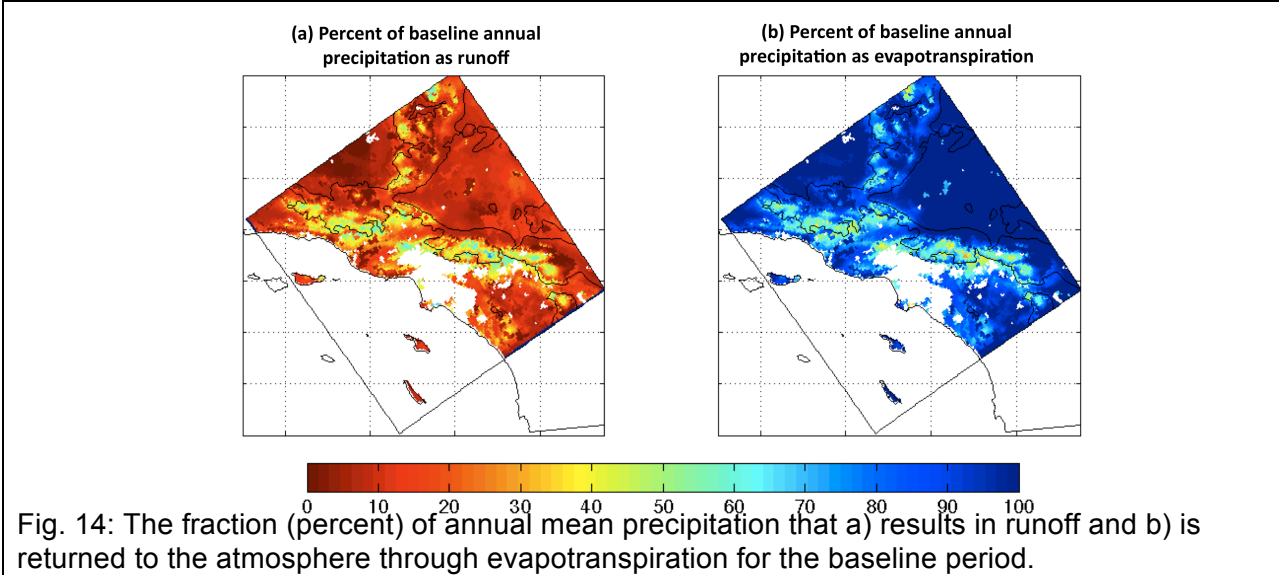
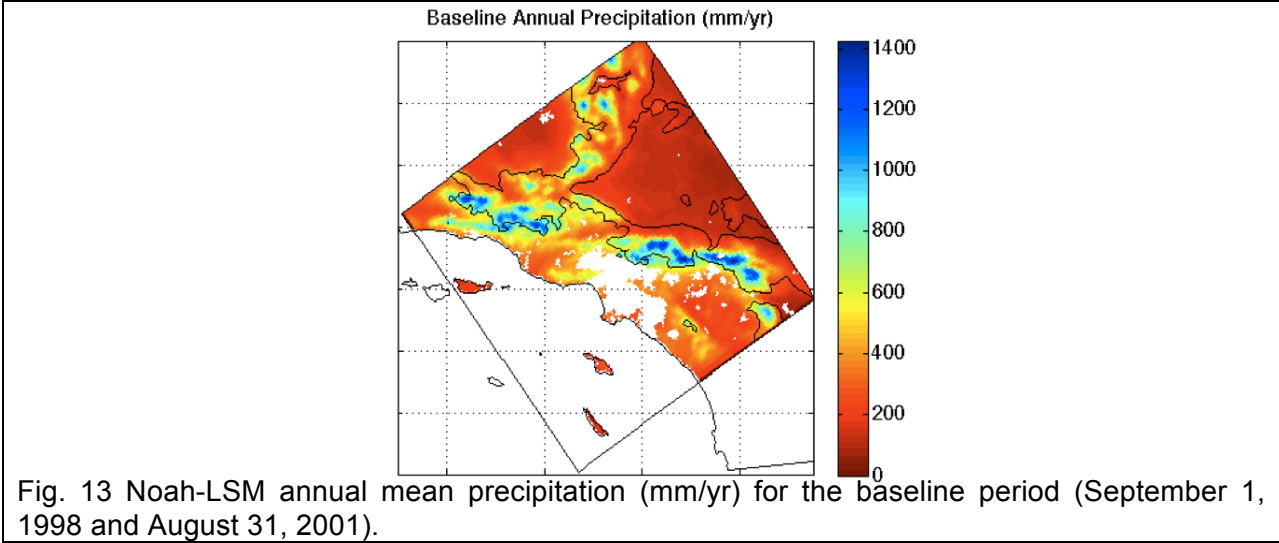


4 Results

In this section, we examine the climatology of surface hydrology in the baseline period as simulated by Noah-LSM by considering the climatological patterns of precipitation, evapotranspiration, runoff, potential evaporation and soil moisture. Then, we examine the climatological differences in surface hydrology between the baseline and future. This is the regional expression of the RCP 8.5 climate change signal that is generated by the dynamically downscaling WRF simulations and used to force the future Noah-LSM simulations. We examine mid-21st century impacts to surface hydrology in the Los Angeles region from Noah-LSM output as forced by five climate change signals: CCSM4 RCP8.5, CNRM-CM5 RCP8.5, GFDL-CM3 RCP8.5, MIROC-ESM-CHEM RCP8.5 and MPI-ESM-LR RCP8.5.

4.1 Climatology of baseline surface hydrology

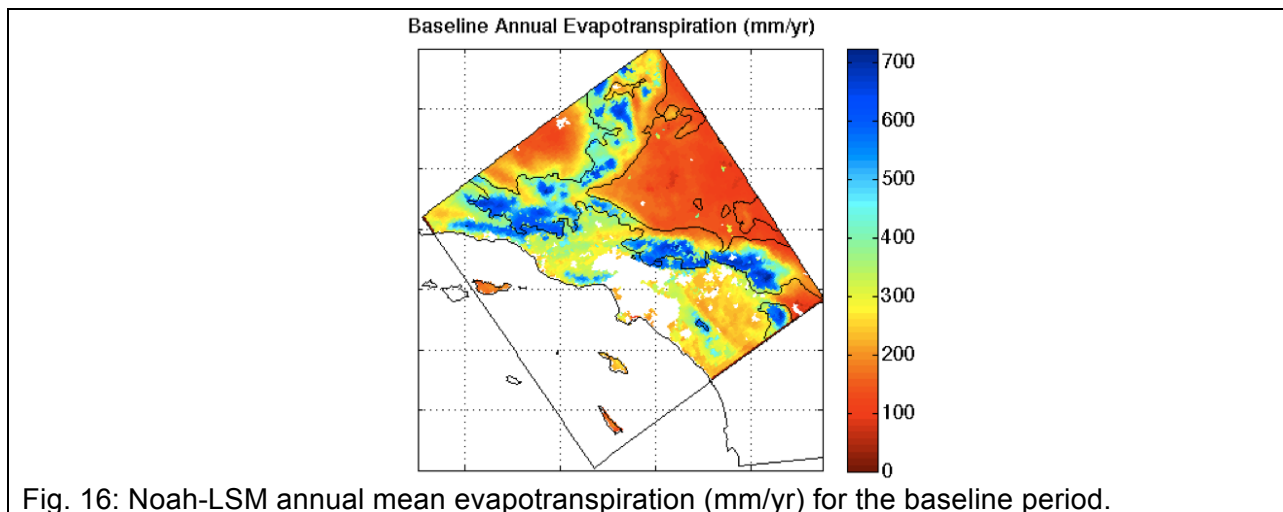
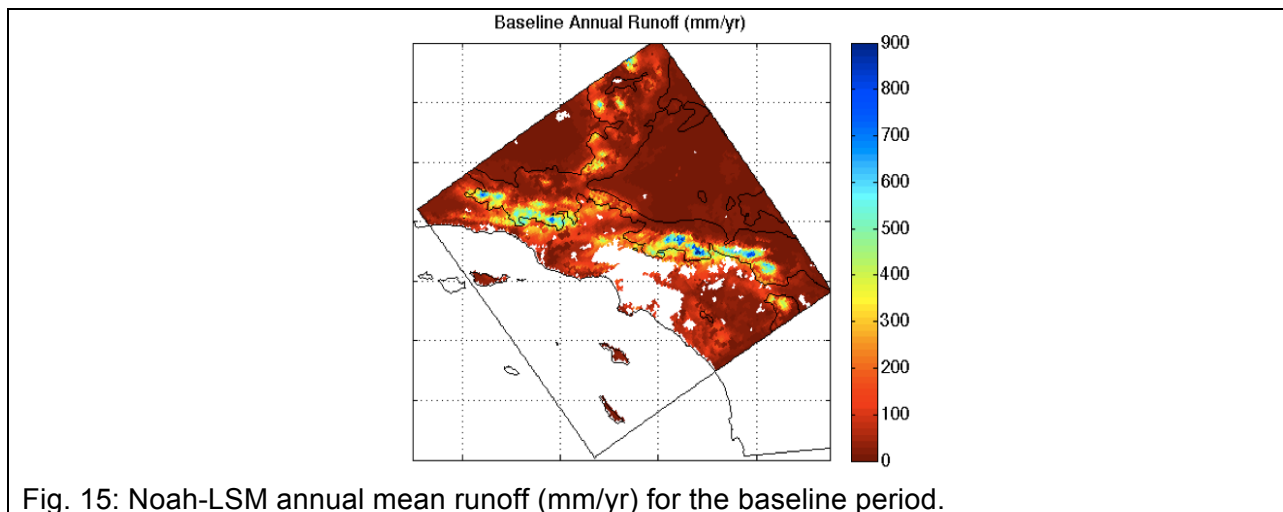
The spatial pattern of climatological precipitation of the baseline period is shown in figure 13. The average annual precipitation (rain plus snow) received at non-urban land points in our study domain is 368mm per year during the baseline period. 91% of our study area's annual precipitation occurs between the months of October and April, and 99.7% of annual precipitation in our study domain falls as rain. On average, the coastal areas of the Los Angeles region experience much more precipitation (375mm per year) than the inland desert region (140 mm per year). Additionally, much precipitation in the region falls in the mountain ranges at elevations higher than 1000m; grid points above 1000m in elevation receive an average of 466mm of precipitation per year, while grid points below 1000m in elevation receive an average of 274mm of precipitation per year in the baseline simulations. In the case of high elevation precipitation, moisture is brought in from the ocean and coastal regions, and then orographic precipitation occurs on the coastal sides of the domain's mountain ranges.



The partitioning of precipitation into runoff and evapotranspiration for the baseline simulation is shown in figure 14. In a semi-arid region like Los Angeles, it appears that precipitation returned to the atmosphere almost entirely through evapotranspiration (as opposed to runoff) in most areas of our study domain. In the inland desert region, 93% of precipitation returns to the atmosphere via evapotranspiration. On the coastal side of high elevation areas (above 1000m, where most precipitation in our study domain falls), 41% of annual precipitation in the baseline period ends up as runoff, while 59% of annual precipitation is lost to evapotranspiration. For low-lying areas (less than 1000m) in the coastal regions of Los Angeles,

83% of annual precipitation is returned to the atmosphere through evapotranspiration, while 17% of precipitation becomes runoff.

The spatial patterns of the climatological runoff and evapotranspiration of the baseline period are shown in figures 15 and 16, respectively. These spatial patterns are obviously well correlated ($>.96$) with the spatial pattern of precipitation in the Los Angeles region, given the lack of routing in Noah-LSM. 83% of annual runoff occurs during the months of December through May. Grid points with elevations under 1000m have 46% less annual runoff than grid points with elevations above 1000m. Moreover, coastal regions have 16% more annual evapotranspiration than inland regions.



We also evaluate patterns of potential evapotranspiration for the baseline period. Potential evapotranspiration represents the atmospheric demand for water from both soil and free water surfaces if sufficient sources were available (Rind et al. 1990). Potential evapotranspiration is estimated by Noah-LSM from the energy available for the vaporization of water assuming no control on the actual availability of water. As a result, potential evapotranspiration serves as an upper bound for actual evapotranspiration rates, and the difference between actual evapotranspiration rates and potential evapotranspiration rates give a sense of the region's aridity. With so much energy available at the surface in this domain, the annual average potential evapotranspiration rate for all non-urban land points is 3140 mm/year. For the inland desert grid points, annual average potential evapotranspiration is 3590 mm/year due to the large moisture deficit of the desert air and energy available for evapotranspiration; for coastal grid points, the average annual evapotranspiration is 2610 mm/year. For our study domain, only 9.5% of potential evapotranspiration is actually evapotranspired, as surface water available for evapotranspiration is severely limited.

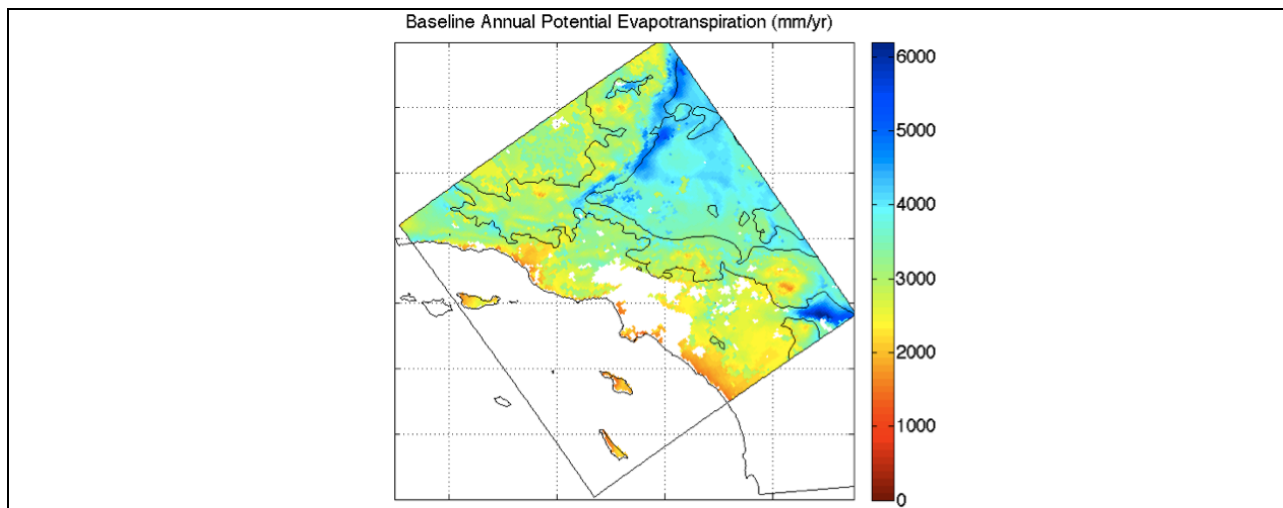
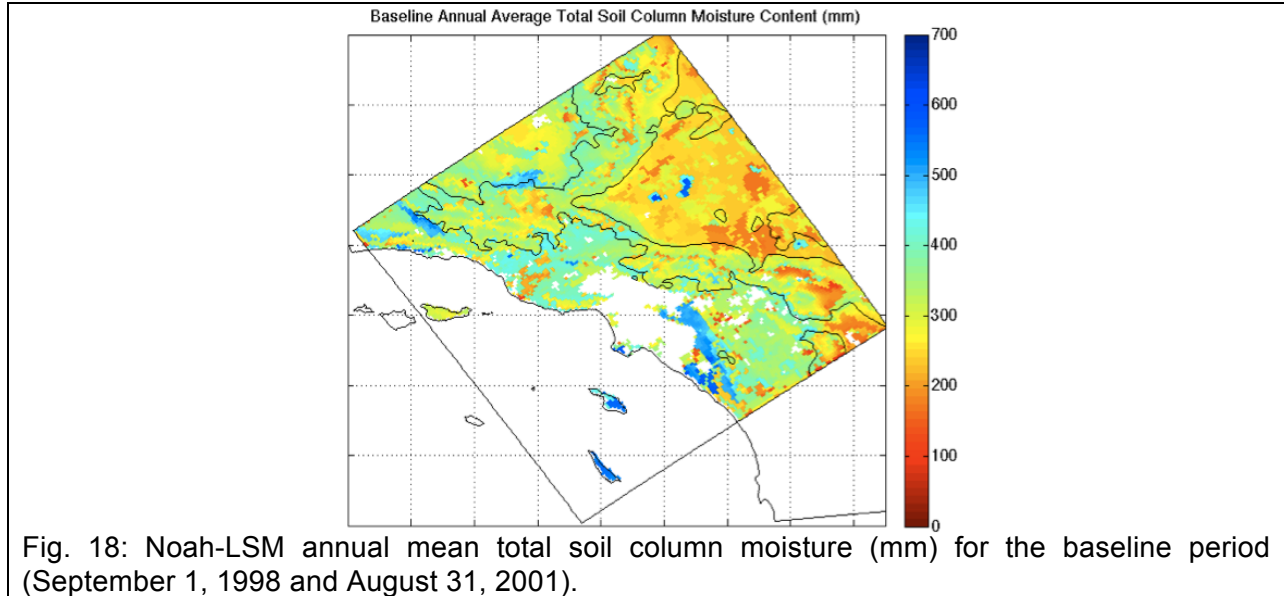


Fig. 17: Noah-LSM annual mean potential evapotranspiration (mm/yr) for the baseline period (September 1, 1998 and August 31, 2001).

Next, we evaluate the average annual total soil column moisture content for the baseline period. The soil column for each grid point in Noah-LSM is 2m deep, and total soil column moisture content includes both liquid and frozen water in the soil column. For the entire domain,

the average annual total soil column moisture content is 326 mm, making the annual soil about 16% saturated. There is a distinct spatial pattern in which the desert soil is significantly drier (270 mm) than the soil of the coastal grid points (370 mm).

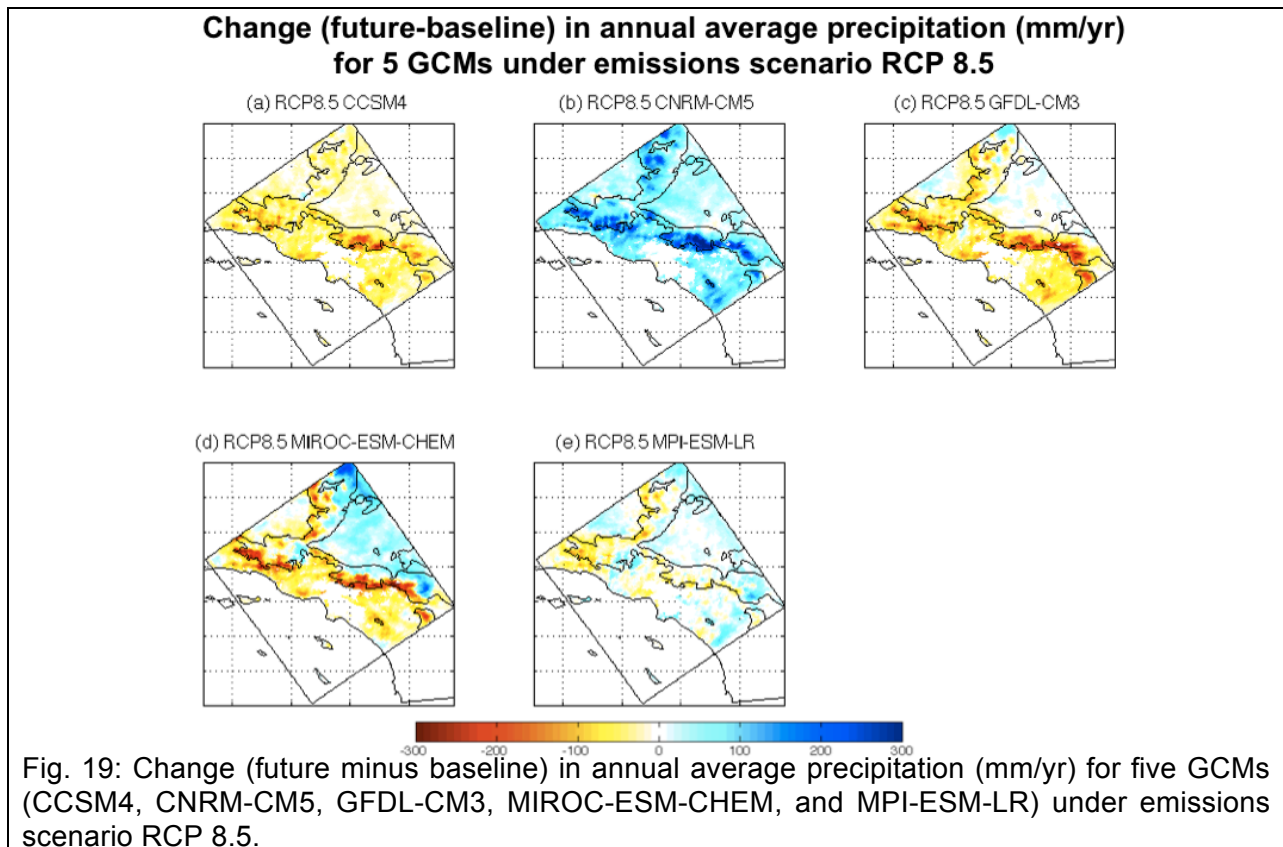


4.2 Changes to annual mean surface hydrological variables

4.2.1 Precipitation

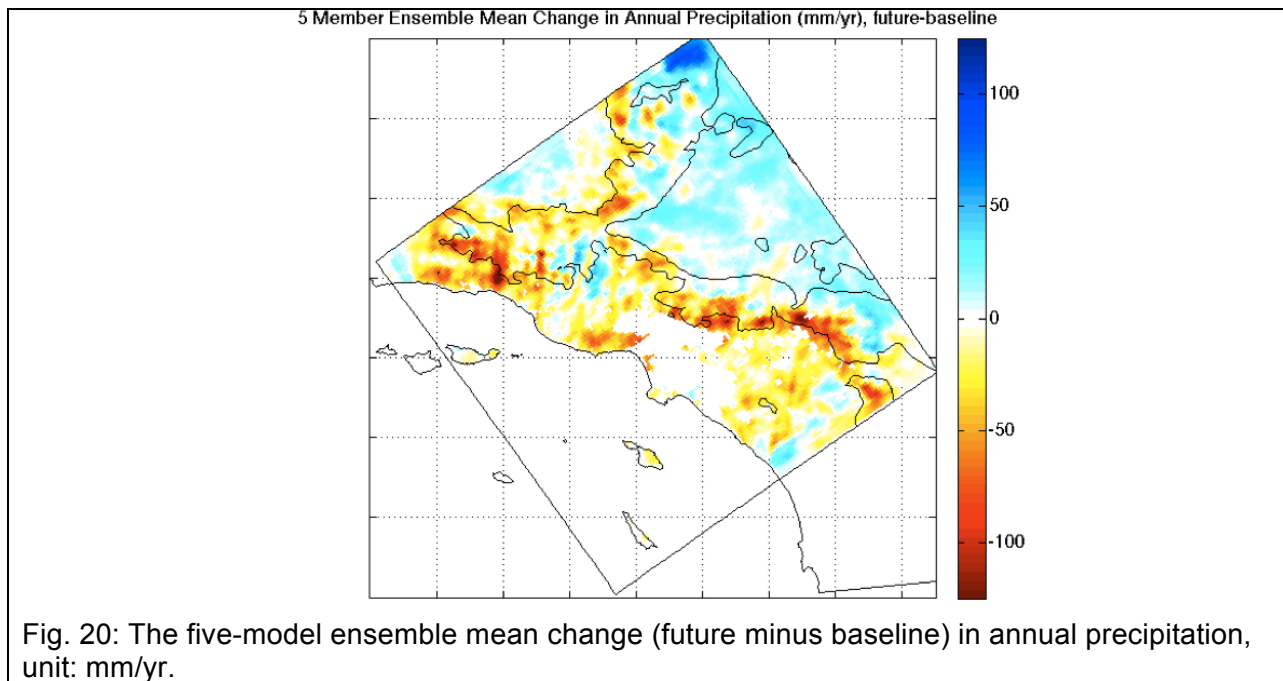
Projections of annual precipitation changes under future emissions scenarios for our study domain are subject to considerable uncertainty. Our domain falls in between the mid-to-high latitudes, which are projected to undergo future increases in annual precipitation, and the sub-tropics, which are projected to undergo future decreases in annual precipitation (Meehl et al. 2007). The location of the Los Angeles region, along with its complex topography and influence by large-scale patterns of natural climate variability (including El Nino/Southern Oscillation and the Pacific Decadal Oscillation), pose problems for future precipitation projections for the region under various climate change scenarios. The change (future-baseline) in annual average precipitation (mm/year) for the five GCMs under emissions scenario RCP 8.5 is seen in figure 19. Of course, there is wide disagreement regarding the sign of the change, which is expected for this region.

CCSM4 and GFDL-CM3 project domain-wide drying (particularly at high elevations), while CNRM-CM5 projects an increase in domain precipitation for the Los Angeles region by the mid-21st century. The sign of the precipitation signal in MIROC-ESM-CHEM and MPI-ESM-LR is not as clear, as areas in the coastal region and on coastal sides of mountains are projected to become drier in the future, while inland and desert regions are projected to become wetter. Despite the difficult nature of projecting precipitation changes for our study domain, it is important to note that any annual precipitation change projected by all GCMs is still within the range of interannual precipitation variability in the baseline simulation.



We interpret the average change in annual precipitation for the five GCMs considered under RCP 8.5 (the “ensemble mean”) as the mostly likely outcome of the change in precipitation, as multi-model ensemble simulations outperform individual model simulations and provide more robust estimates of future climate change and uncertainties. The ensemble mean

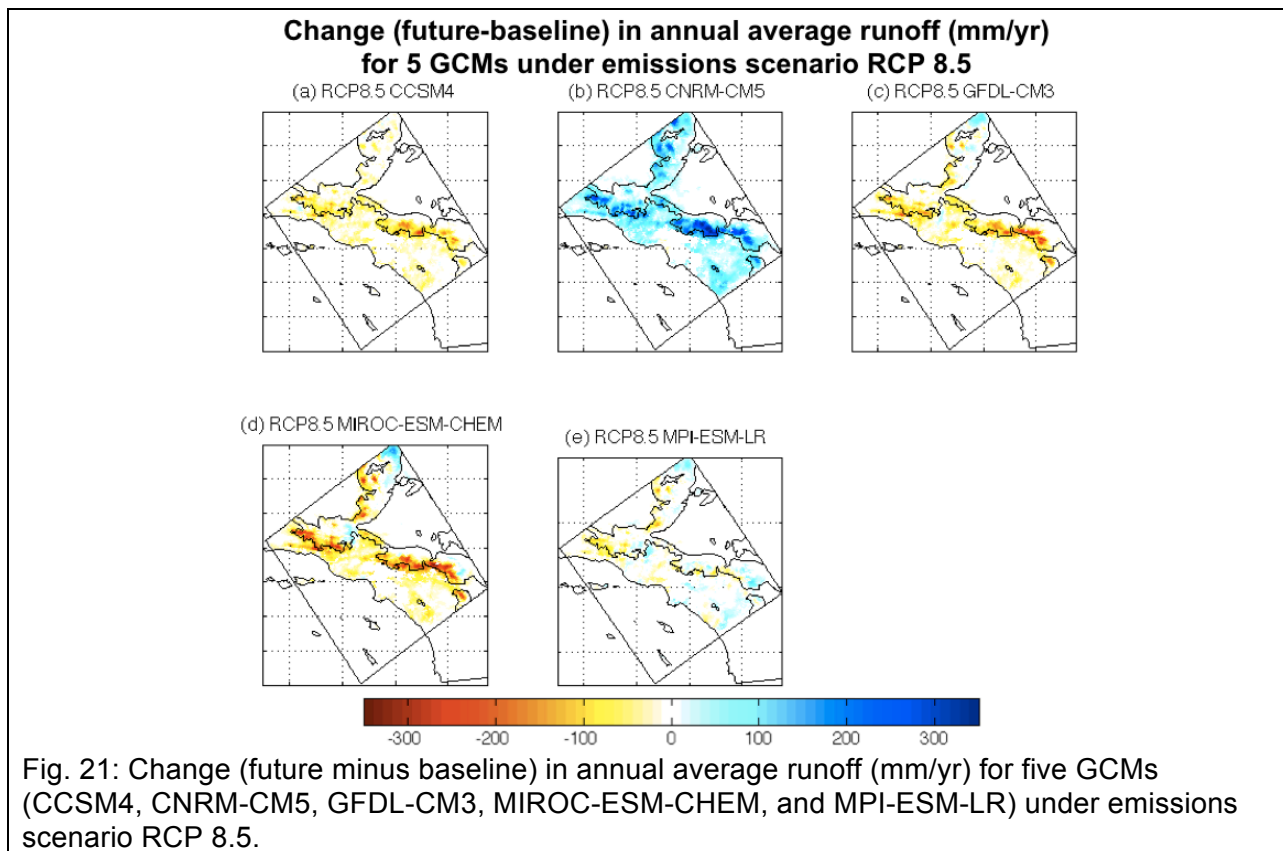
annual-mean precipitation change (future minus baseline) for the five-member model ensemble is shown in figure 20. A distinct spatial pattern emerges from the ensemble mean, in which coastal grid points and the coastal side of high-elevation grid points are projected to undergo decreases in precipitation by the mid-21st century, while the inland and desert regions are expected to experience future increases in precipitation. The annual precipitation of coastal grid points, as simulated by the ensemble-mean, is projected to decrease by 17.5mm/year by the mid 21st century. On the other hand, the annual precipitation of inland grid points in the high deserts, as simulated by the ensemble-mean, is projected to increase by a mere 2mm/year by the mid 21st century.



4.2.2 Runoff

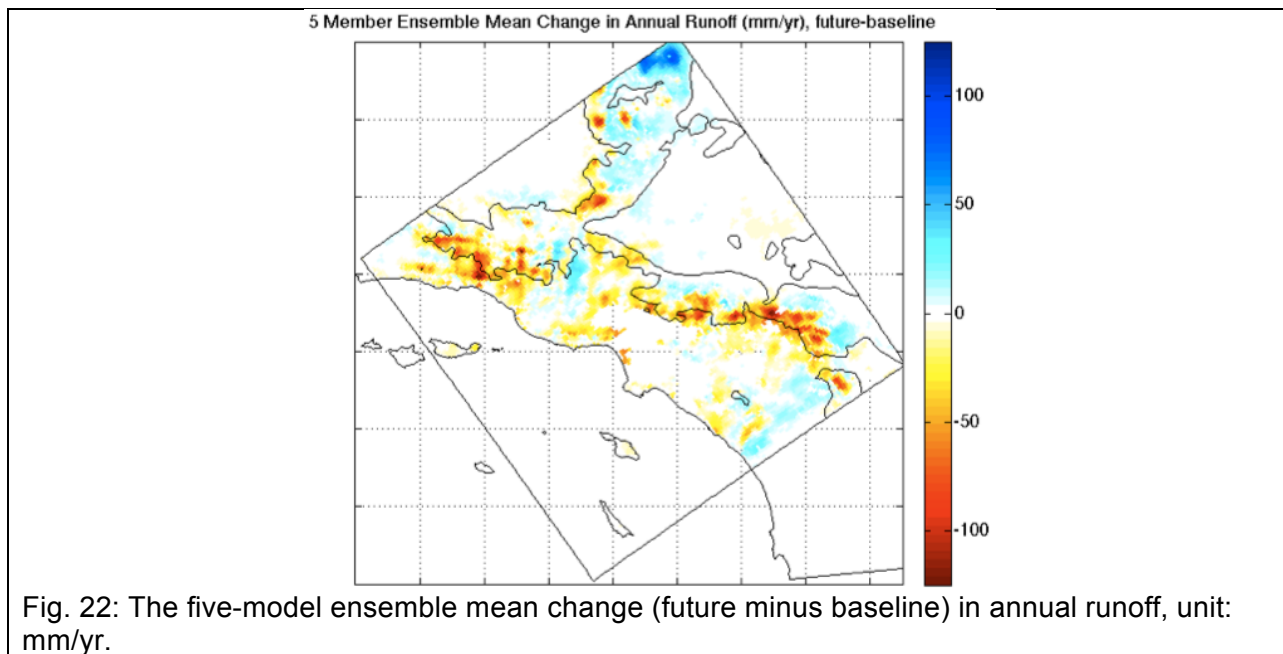
The change (future-baseline) in annual average runoff (mm/year) that results from the change in annual precipitation for five GCMs under RCP 8.5 is seen in figure 21. Changes in annual average runoff are particularly noticeable in the coastal and mountain regions. The sign of the change in annual runoff for each gridpoint in each GCM heavily depends on the sign of the change in annual precipitation as projected by that GCM, with a correlation coefficient above

.88 for all models. Grid points that are projected to undergo future increases in precipitation are projected to experience similar increases in runoff, and grid points that are projected to undergo future decreases in precipitation are projected to experience similar decreases in runoff. For all future simulations in Noah-LSM, the sign of the change in annual runoff is the same as the sign of the change in annual precipitation for over 97% grid points in our domain. Thus, the change in precipitation seems to control the change in runoff in our simulation domain.



The ensemble mean change (future minus baseline) in annual runoff for the five-member model ensemble is shown in figure 22. Again, the sign of the change in annual runoff as simulated by the ensemble-mean is the same as the sign of the change in precipitation for 95% of non-urban land points in our domain, with a high correlation between the two changes (.91). According to the ensemble mean, coastal grid points will undergo an average decrease of 8 mm/year of runoff, while inland desert grid points are projected to experience nearly no change in annual runoff. Some areas above 1000m in elevation on the coastal side of the mountain

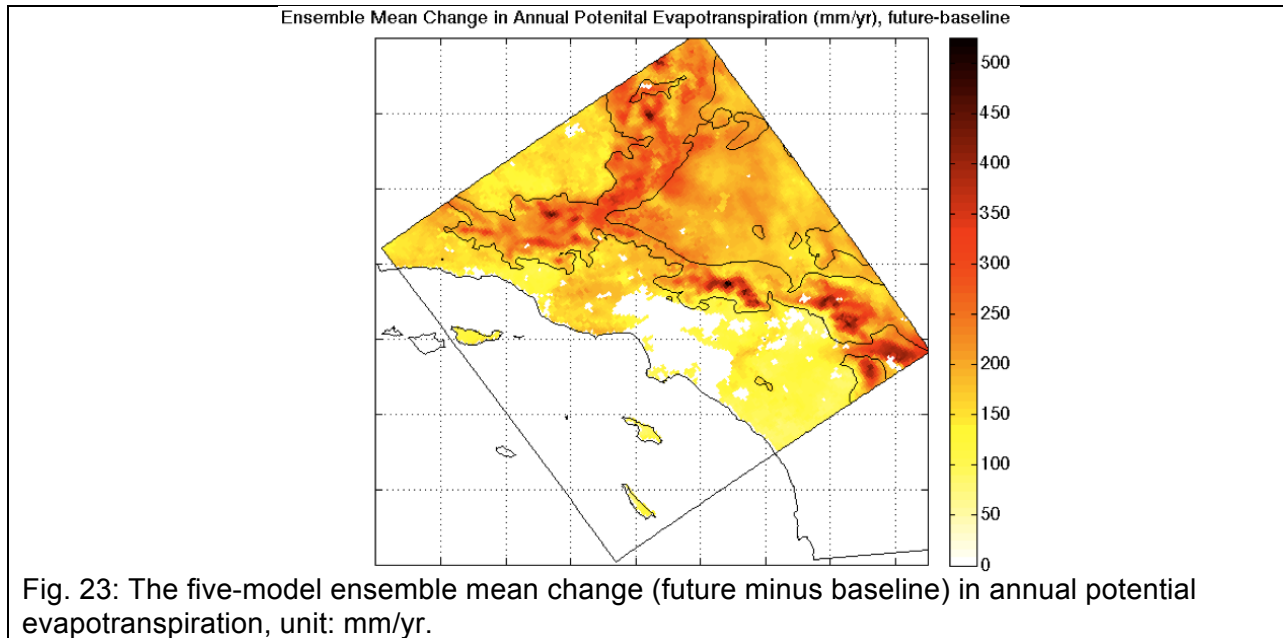
ranges are projected to experience decreases in annual runoff as strong as 130 mm/year, posing serious concerns for water resources and availability. While the ensemble mean may be a better representative of future precipitation changes because it eliminates the uncertainty associated with biases in individual GCMs, the individual models hardly agree on the sign of precipitation changes and the magnitude of the ensemble mean change in precipitation is considerably smaller than that of all models. Thus, we should analyze ensemble mean changes cautiously in this assessment.



4.2.3 Evapotranspiration

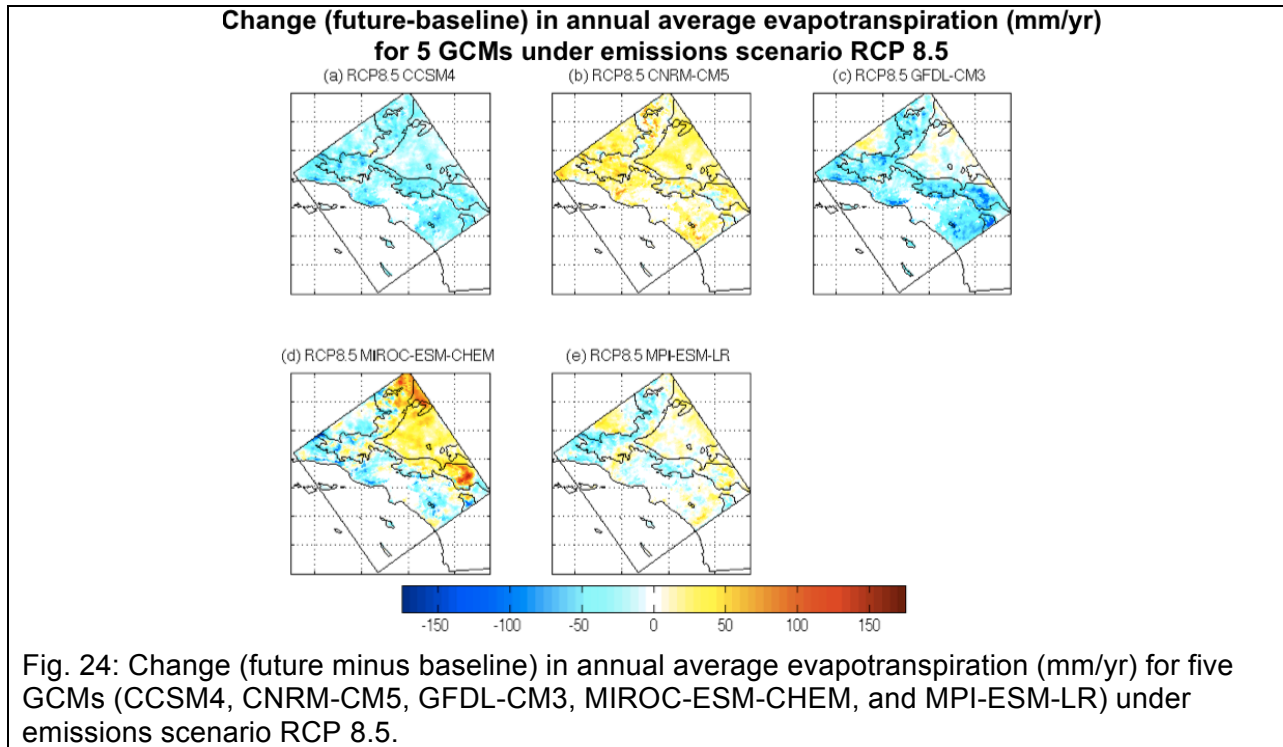
Future changes to evapotranspiration are of particular interest to water planners due to the impact of evapotranspiration on water availability. Under RCP 8.5 for each future simulation, incoming long wave radiation increases due to the increase in concentration of greenhouse gases in the atmosphere. In turn, this provides more energy to the surface, which increases the potential evapotranspiration rate throughout the domain. The ensemble mean change in annual potential evapotranspiration (future minus baseline) for the five-member model ensemble is shown in figure 23. Each future simulation projects domain-wide increases in potential

evapotranspiration for all grid points, with an average increase of 180 mm/year in potential evapotranspiration. Increases in potential evapotranspiration are highest at elevations above 1000m, where decreases in snow cover and albedo during the winter months allow more energy to reach the surface, thus providing more energy for potential evapotranspiration. The ensemble mean serves as a good indication of future changes in annual potential evapotranspiration.

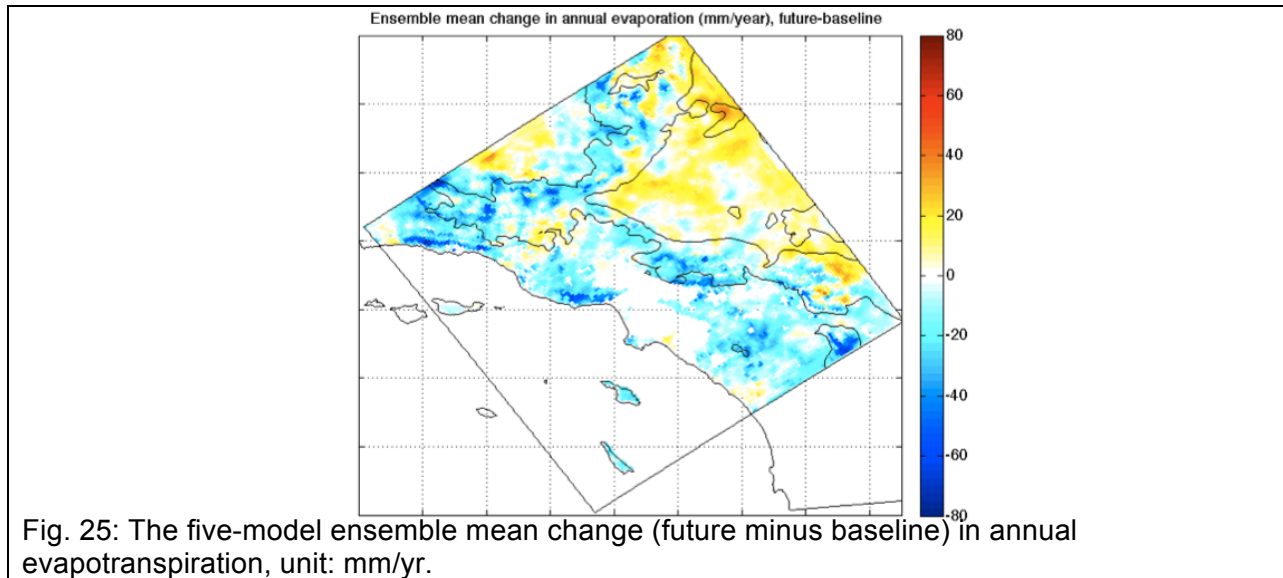


Of course, while annual potential evapotranspiration is expected to increase in a warmer, more energized future, actual evapotranspiration rates are limited by surface water availability. The change (future-baseline) in annual average evapotranspiration (mm/year) as projected by five GCMs under RCP 8.5 is seen in figure 24. The relationship between the change in annual precipitation and change in annual evapotranspiration is not as well defined as the relationship between the change in annual precipitation and change in annual runoff, where the sign of both changes was nearly always the same for grid points. While decreased precipitation (for example, as projected in the RCP 8.5 CCSM4 simulation) often implies less water available for evapotranspiration (and hence a corresponding decrease in

evapotranspiration, as projected by CCSM4), the future runs do simulate some regions that experience decreases in precipitation yet increases in evapotranspiration.



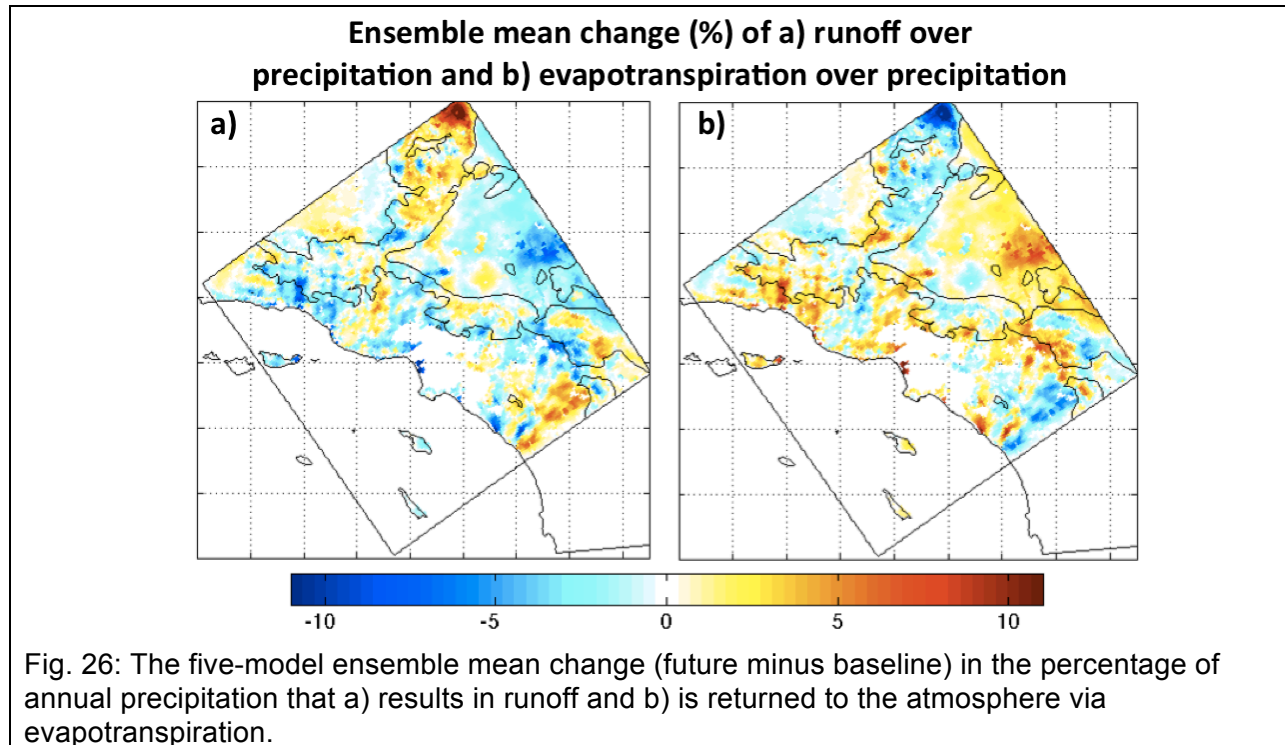
The ensemble mean change (future minus baseline) in annual evapotranspiration for the five-member model ensemble is shown in figure 25. Overall, widespread decreases in evapotranspiration are expected in coastal regions, with an average decrease in evapotranspiration of 13 mm/year. This is likely due to the projected decrease in precipitation for this region, which decreases the water available for actual evapotranspiration despite increased energy for higher potential evapotranspiration. In the inland desert regions, the ensemble mean projects a precipitation increase of 2 mm/yr, which is accompanied by a slight increase in inland desert evapotranspiration of 1 mm/yr.



4.2.4 Fractions of evaporation over precipitation and runoff over precipitation

To examine changes to the partitioning of precipitation once it reaches the surface, we can examine changes to the fraction of evaporation of precipitation and the fraction of runoff over precipitation. Figure 26 shows the five-model ensemble mean change (future minus baseline) in the percentage of annual precipitation that results in runoff and the percentage of annual precipitation that is returned to the atmosphere through evapotranspiration. Of course, because Noah-LSM output satisfies the surface water balance equation, the changes to these percentages are nearly the same in magnitude and always opposite in sign. No robust domain-wide change in either percentage is observed, implying the domain does not shift to become more runoff-dominated or evapotranspiration-dominated. As the five-model ensemble mean project evapotranspiration increases in the inland desert regions, the percent of evapotranspiration over precipitation for that region increases by an average of 2.1%. Averaged over the entire study domain, however, the percent of evapotranspiration over precipitation only increases by .5%, a fractional change. Unfortunately, the multi-model ensemble mean may not be a good indication of likely changes to the fractions of evaporation

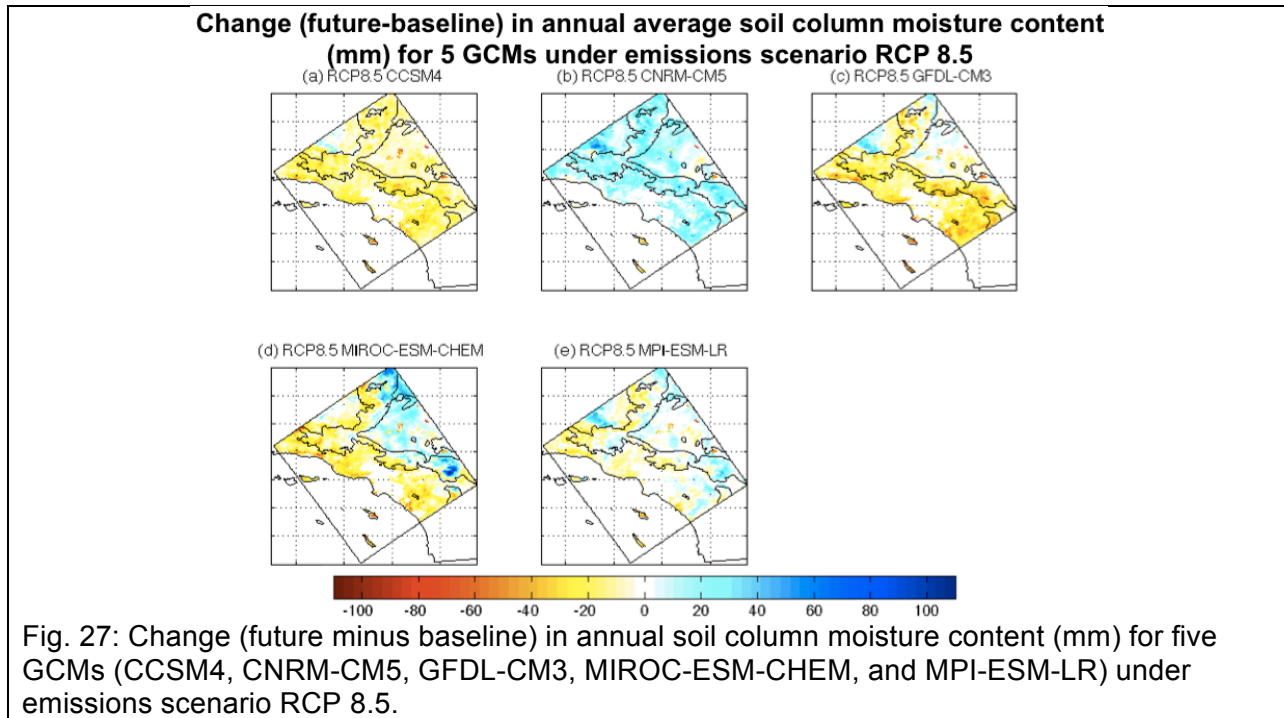
over precipitation and runoff over precipitation, as the change for each individual model is so dependent on the model's initial change in precipitation.



4.2.5 Soil Column Moisture Content

The change (future-baseline) in annual average soil column moisture content (mm) as projected by five GCMs under RCP 8.5 is seen in figure 24. Unsurprisingly, the change in soil column moisture content is highly correlated (.98) to the change in precipitation, with the sign of the precipitation change being the same as the sign of the soil column moisture content change for over 98% of gridpoints. The ensemble mean domain-average change in soil column moisture content is marginal decrease of 6mm (out of a 2000mm soil column). While the change in annual average soil column moisture content for individual models may have distinct coastal vs. inland desert differences (for example in the RCP 8.5 MIROC-ESM-CHEM simulation), no distinct spatial pattern emerges in the ensemble-mean change in soil column moisture content. There is simply a widespread weak drying of the soil, which is nearly negligible for the 2m soil column. Perhaps this is due to the fact that in the ensemble mean, regions that are

projected to undergo increases in precipitation are expected to also undergo increases in evapotranspiration of a similar magnitude (thus not allowing the soil moisture to change much), and regions that are projected to undergo decreases in precipitation are expected to also undergo decreases in evapotranspiration of a similar magnitude (thus also now allowing the soil moisture to change much).



5 Discussion and Summary

The current study refines our understanding of changes to surface hydrology in the Los Angeles region under a “business as usual” emissions scenario for the mid 21st century. Our goal was to quantify and describe potential impacts of climate change to precipitation, runoff, evapotranspiration and soil column moisture content in the Los Angeles region, as little previous research has focused on the impacts of climate change to water resources and surface hydrology in the southern regions of California.

The methods presented in our study provide an approach to evaluate high-resolution changes to surface hydrological fluxes and states under future climate change for the Los Angeles region. Using, WRF, we dynamically downscaled coarse-resolution reanalysis data and future GCM simulation output to model atmospheric dynamics in our study domain at 2km resolution. Then, we used WRF output as the forcing for our baseline and future Noah-LSM simulations, which output near-surface state variables and surface turbulent fluxes. This methodology allowed us to assess potential impacts of climate change to surface hydrology in the Los Angeles region at scales relevant to local policy makers or water resources planners.

By comparing observed variations related to surface hydrology to Noah-LSM output, we are able to evaluate model performance. We validate Noah-LSM model performance for the baseline period by comparing simulated output of soil temperature, evapotranspiration and runoff to observational point measurements from the CIMIS weather stations and USGS HCDN-2009 streamflow gauges. Additionally, we discuss the validation of dynamically downscaled WRF output for the baseline simulation. Our validation exercise (section 3) showed that the seasonal cycles of surface hydrological and meteorological variables as simulated by Noah-LSM are very much consistent with observational measurements.

While this research sheds light on climate change impacts to surface hydrology in the Los Angeles region, there is certainly room for future research and expansion. The uncertainty

associated with our choice of GCMs from the CMIP5 data archive may cause the ensemble mean in our results to be a poor representation of central tendencies. While multi-model ensemble mean simulations typically outperform individual model simulations and provide more robust estimates of future climate change, the ensemble mean does not seem to be a good indicator of changes to surface hydrology in the Los Angeles region for the mid 21st century. The choice of the five GCMs we dynamically downscaled through WRF heavily influenced the change in precipitation for our study domain, which in turn deeply impacted the changes to surface hydrological fluxes and states. Unfortunately, the changes in runoff, evapotranspiration and soil column moisture content that result from changes to precipitation are too highly dependent on the sign of the change in precipitation for that model.

Resampling techniques, in which we estimate the precision of the ensemble mean statistics by using subsets of the Noah-LSM model (for example, a four-member ensemble mean as opposed to a five-member ensemble mean), produced significantly different statistics for the ensemble mean changes to surface hydrology. Perhaps the five-member ensemble mean we selected does not provide a robust understanding of changes (both magnitude and sign) to surface hydrology of Los Angeles for the mid 21st century, simply due to the choice of GCMs. Because it would be extremely time-consuming and computationally expensive to force Noah-LSM with dynamically downscaled output from every GCM in the CMIP5 data archive, we must develop techniques that allow us to better characterize and quantify future changes to surface hydrology in the Los Angeles region and the associated uncertainty.

Perhaps statistical downscaling can be employed to more quickly produce the meteorological forcing variables for Noah-LSM for more GCMs in the CMIP5 data archive under various emissions scenarios; this could help account for the considerable uncertainty associated with a limited choice of GCMs and only one emissions scenario (or representative concentration pathway). This could help better quantify and describe potential impacts of climate change to precipitation, runoff, evapotranspiration and soil column moisture content in the Los Angeles

region. This information could be used by local water resource managers to make Los Angeles' water system and sources less vulnerable to impacts of climate change.

6 References

- Allen, R.G., L.S. Pereira, D. Raes, M. Smith, 1998: Crop evapotranspiration. Guidelines for computing crop requirements. Irrigations and Drainage Paper 56. FAO, Rome.
- Allen, R.G., W.O Pruitt, J.L. Wright, T.A. Howell, F. Ventura, R. Snyder, D. Itenfisu, P. Steduto, J. Berengena, J.B. Yrisarry, M. Smith, L.S. Pereira, D. Raes, A. Perrier, I. Alves, I. Walter, R. Elliott, 2006: A recommendation on standardized surface resistance for hourly calculation of reference ETO by FAO56 Penman-Monteith method. *Agricultural Water Management*. 81, 1-22.
- Berg, N., A. Hall, F. Sun, and S. Capps, 2013: Mid 21st Century Precipitation Changes Over the Los Angeles Region. Unpublished manuscript.
- Brutsaert, W., 2005. *Hydrology: An Introduction*. New York: Cambridge University Press.
- Caldwell, P., H.N.S. Chin, D.C. Bader, and G. Bala, 2009: Evaluation of a WRF dynamical downscaling simulation over California. *Climatic Change*, 95, 499-521.
- Cayan, D.R., 1996: Interannual climate variability and snowpack in the western United States. *Journal of Climate*, 9, 928-948.
- Cayan, D. R., S. A. Kammerdiener, M.D. Dettinger, J.M. Caprio, D.H. Peterson, 2001: Changes in the onset of spring in the western United States. *Bulletin of the American Meteorological Society*, 82, 399–415.
- Chen, F., K. Mitchell, J. Schaake, Y. Xue, H. Pan, V. Koren, Y. Duan, M. Ek, A. Betts, 1996: Modeling of land surface evaporation by four schemes and comparison with FIFE observations. *Journal of Geophysical Research*, 101, 7251–7268.
- Chen, F., J. Dudhia, 2001: Coupling an advanced land-surface/hydrology model with the Penn State/NCAR MM5 modeling system. Part I: Model implementation and sensitivity. *Monthly Weather Review*, 129, 569–585.

- Chen, F., K.W. Manning, M.A. LeMone, S.B. Trier, J.G. Alfieri, R. Roberts, J. Wilson, M. Tewari, D. Niyogi, T.W. Horst, S.P. Oncley, J.B. Basara, P.D. Blanken, 2007: Evaluation of the characteristics of the NCAR high-resolution land data assimilation system during IHOP_2002. *Journal of Applied Meteorology and Climatology*, 46, 694–713.
- Christensen, N.S., A.W. Wood, N. Voisin, D.P. Lettenmaier, and R.N. Palmer, 2004: The Effects of Climate Change on the Hydrology and Water Resources of the Colorado River Basin. *Climatic Change* 62(1-3): 337-363.
- Clapp, R.B., G.M. Hornberger, 1978: Empirical equations for some soil hydraulic properties. *Water Resources Research*, 14(4), 601.
- Conil S., A. Hall, 2006: Local regimes of atmospheric variability: A case study of Southern California. *Journal of Climate*, 19, 4308-4325.
- Cox, P.M., R.A. Betts, C.D. Jones et al., 2000: Acceleration of global warming due to carbon-cycle feedbacks in a coupled climate model. *Nature*, 408(6809), 184–187.
- Dettinger, M.D., and D.R. Cayan, 1995: Large-scale atmospheric forcing of recent trends toward early snowmelt runoff in California. *Journal of Climate*, 8, 606–623.
- Dudhia, J., 1989: Numerical study of convection observed during the winter monsoon experiment using a mesoscale two-dimensional model. *Journal of the Atmospheric Sciences*, 46, 3077-3107.
- Ek, M. B., K. E. Mitchell, Y. Lin, E. Rogers, P. Grunmann, V. Koren, G. Gayno, J.D. Tarpley, 2003: Implementation of Noah land surface model advances in the National Centers for Environmental Prediction operational mesoscale Eta model. *Journal of Geophysical Research*, 108 (D22), 8851.
- Giorgi, F., L.O. Mearns, 1991: Approaches to the simulation of regional climate change: a review. *Reviews of Geophysics*, 29, 191–216.
- Giorgi, F., B. Hewitson, J. Christensen, M. Hulme, H. von Storch, P. Whetton, R. Jones, L. Mearns and C. Fu, 2001: Regional climate information – evaluation and projections. In:

- J.T. Houghton, Y. Ding, D.J. Griggs, M. Noguera, P.J. van der Linden, X. Dai, K. Maskell and C.A. Johnson (eds.). pp. 583–638. *Climate Change 2001: The Scientific Basis. Contribution of Working Group I to the Third Assessment Report of the Intergovernmental Panel on Climate Change*. Cambridge University Press.
- Gleckler, P. J., K. E. Taylor, and C. Doutriaux, 2008: Performance metrics for climate models, *Journal of Geophysical Research*, 113, D06104.
- Gleick, P.H., and E.L. Chalecki, 1999: The Impacts of Climate Changes for Water Resources of the Colorado and Sacramento-San Joaquin River Basins. *Journal of the American Water Resources Association*, 35(6), 1429-1441.
- Golubev, V. S. et al., 2001: Evaporation changes over the contiguous United States and the former USSR: a reassessment. *Geophysical Research Letters*, 28(13), 2665-2668.
- Hall, A.D, et al, 2012: Mid-Century Warming the in the Los Angeles Region. Available at <http://c-change.la/pdf/LARC-web.pdf>.
- Hart, Q.J, M. Brugnach, B. Temesgen, C. Ruesa, S.L Ustin, K. Frame, 2008. Daily reference evapotranspiration for California using satellite imagery and weather station measurement interpolation. *Civil Engineering and Environmental Systems*, 26 (1), 19-33.
- Hayhoe, K., D.R. Cayan, C.B. Field, P.C. Frumhoff, E.P. Maurer, N.L. Miller, S.C. Moser, S.H. Schneider, K.N. Cahill, E.E. Cleland, L. Dale, R. Drapek, R.M. Hanemann, L.S. Kalkstein, J. Lenihan, C.K. Lunch, R.P. Neilson, S.C. Sheridan, J.H. Verville, 2004: Emissions Pathways, Climate Change, and Impacts on California. *Proceedings of the National Academy of Sciences of the United States of America*, 101(34), 12422-12427.
- Hogue, T. S., 2003: A multi-criteria evaluation of land-surface models and application to semi-arid regions. Ph.D. dissertation, The University of Arizona, 247 pp.
- Hogue, T. S., L. Bastida, H. Gupta, S. Sorooshian, K. Mitchell, W. Emmerich, 2005: Evaluation and Transferability of the Noah Land Surface Model in Semiarid Environments. *Journal of Hydrometeorology*, 6, 68-84.

- Hong, S.-Y., Y. Noh, J. Dudhia, 2006: A new vertical diffusion package with an explicit treatment of entrainment processes. *Monthly Weather Review*, 134, 2318-2341.
- Hughes M., A. Hall, R.G. Fovell, 2007: Dynamical controls on the diurnal cycle of temperature in complex topography. *Climate Dynamics*, 29, 277-292.
- Intergovernmental Panel on Climate Change (IPCC) (2007) Synthesis report, Contribution of Working Groups I, II and III to the Fourth Assessment Report of the Intergovernmental Panel on Climate Change Core Writing Team. In: Pachauri RK, Reisinger A (eds) IPCC, Geneva, Switzerland, pp 104.
- Jarvis, P.G., 1976: The interpretation of leaf water potential and stomatal conductance found in canopies of the field. *Philosophical Transactions of the Royal Society of London*, 273 (927), 593-610.
- Jin, J., N. L. Miller, 2007: Analysis of the Impact of Snow on Daily Weather Variability in Mountainous Regions Using MM5, *Journal of Hydrometeorology*, 8, 245-258.
- Jones, R.G., J.M. Murphy, M. Noguer, A.B. King, 1997: Simulation of climate change over Europe using a nested regional climate model. Comparison of driving and regional model responses to a doubling of carbon dioxide concentration. *Quarterly Journal of the Royal Meteorological Society*, 123 (538), 265–292.
- Jung, M., M. Reichstein, P. Ciais et al., 2010: Recent decline in the global land evapotranspiration trend due to limited moisture supply. *Nature*, 467(7318), 951–954.
- Kain, J. S., 2004: The Kain-Fritsch convective parameterization: An update. *Journal of Applied Meteorology*, 43 (1), 170-181.
- Kanamitsu, M., and H. Kanamaru, 2007: Fifty-seven-year California reanalysis downscaling at 10 km (CaRD10). Part I: system detail and validation with observations. *Journal of Climate*, 20 (22), 5553–5571.
- Kapnick, S. and A. Hall, 2010: Observed climate-snowpack relationships in California and their implications for the future. *Journal of Climate*, 23 (13), 3446-3456.

- Klein, S.A., D.L. Hartmann, 1993: The seasonal cycle of low stratiform clouds. *Journal of Climate*, 6, 1587-1606.
- Knowles, N., M.D. Dettinger, D.R. Cayan, 2006: Trends in snowfall versus rainfall in the western United States. *Journal of Climate*, 19, 4545–4559.
- Leung, L.R., Y. Qian, X. Bian, 2003: Hydroclimate of the western United States based on observations and regional climate simulations of 1981-2000. Part I: seasonal statistics. *Journal of Climate*, 16, 1892-1911.
- Leung L.R., Y. Qian, X. Bian, W.M. Washington, J. Han, J. Roads, 2004: Mid-century ensemble regional climate change scenarios for the western United States. *Climatic Change* 62, 75–113.
- Levien, L., C. Fischer, S. Parks, B. Maurizi, J. Suero, L. Mahon, P. Longmire, and P. Roffers, 2002: Monitoring land cover changes in California, a USFS and CDF cooperative program, South Coast Project Area. State of California, Resources Agency, Department of Forestry and Fire Protection, Sacramento, CA.
- Lin, Y.-L., R. D. Farley, H. D. Orville, 1983: Bulk parameterization of the snow field in a cloud model. *Journal of Applied Meteorology*, 22, 1065-1092.
- Lins, H.F., 2012, USGS Hydro-Climatic Data Network 2009 (HCDN–2009): U.S. Geological Survey Fact Sheet 2012–3047, 4 p., available only at <http://pubs.usgs.gov/fs/2012/3047/>.
- Mahrt, L., H.-L. Pan, 1984, A two-layer model of soil hydrology, *Boundary Layer Meteorology*, 29, 1– 20.
- Meehl, G., T. F. Stocker, W. Collins, and coauthors, 2007: Global climate projections. *Climate Change 2007: The Physical Science Basis. Contribution of Working Group I to the Fourth Assessment Report of the Intergovernmental Panel on Climate Change*, S. Solomon, D. Qin, and M. Manning, Eds., Cambridge University Press, Cambridge and New York, 996pp.

- Meinshausen, M., S. J. Smith, K. V. Calvin, J. S. Daniel, M. Kainuma, J.-F. Lamarque, K. Matsumoto, S. A. Montzka, S. C. B. Raper, K. Riahi, A. M. Thomson, G. J. M. Velders, D. van Vuuren, 2011: The RCP Greenhouse Gas Concentrations and their Extension from 1765 to 2300. *Climatic Change (Special Issue)*, 109, 213-241.
- Miller, D. A., R. A. White RA, 1998: A conterminous United States multilayer soil characteristic data set for regional climate and hydrology modeling. *Earth Interactions*, 2, 1-26.
- Mitchell, K.E., D. Lohmann, P. R. Houser, E. F. Wood, J. C. Schaak, A. Robock, B. A. Cosgrove, J. Sheffield, Q. Duan, L. Luo, R. W. Higgins, R. T. Pinker, J. D. Tarpley, D. P. Lettenmaier, C. H. Marshall, J. K. Entin, M. Pan, W. Shi, V. Koren, J. Meng, B. H. Ramsay, A. A. Bailey, 2004: The multi-institutional North American Land Data Assimilation System (NLDAS): Utilizing multiple GCIP products and partners in a continental distributed hydrological modeling system. *Journal of Geophysical Research*, 109, D07S90.
- Mlawer, E. J., S. J. Taubman, P. D. Brown, M. J. Iacono, S. A. Clough, 1997: Radiative transfer for inhomogeneous atmosphere: RRTM, a validated correlated-k model for the long-wave, *Journal of Geophysical Research*, 102 (D14), 16663-16682.
- Moss, R. H., et al., 2010: The next generation of scenarios for climate change research and assessment, *Nature*, 463, 747–756.
- Mote ,P.W., A.F. Hamlet, M.P. Clark, and D.P. Lettenmaier, 2005: Declining mountain snowpack in western North America. *Bulletin of the American Meteorological Society*, 86, 39-49.
- Mote, P.W., and E.P. Salathe, 2010: Future climate in the Pacific Northwest. *Climatic Change*, 102, 29-50.
- Mote, P.W., 2003: Trends in snow water equivalent in the Pacific Northwest and their climatic causes. *Geophysical Research Letters*, 30, 1601.

- Pan, L.-L., S.-H. Chen, D. Cayan, M.-Y. Lin, Q. Hart, M.-H. Zhang, Y. Liu, J. Wang, 2011: Influences of climate change on California and Nevada regions revealed by a high-resolution dynamical downscaling study. *Climate Dynamics*, 37, 2005-2020.
- Peters-Lidard, C. D., et al., 2007: High performance Earth system modeling with NASA/GSFC's Land Information System. *Innovations in Systems and Software Engineering*, 3(3), 157–165.
- Peterson, T. C., V.S. Golubev, and P.V. Groisman, 1995: Evaporation losing its strength. *Nature*, 377, 687–688.
- Qian, Y., S.J. Ghan, L.R. Leung, 2009: Downscaling hydroclimatic changes over the Western U.S. Based on CAM subgrid scheme and WRF regional climate simulations, *International Journal of Climatology*, 30, 675-693.
- Richards, L.A., 1931: Capillary conduction of liquids through porous mediums. *Physics*, 1 (5), 318–333.
- Rind, D., R. Goldberg, J. Hansen, C. Rosenzweig, and R. Ruedy, 1990: Potential evapotranspiration and the likelihood of future drought. *Journal of Geophysical Research*, 95, 9983-10004.
- Roderick, M. L., and G.D. Farquhar, 2002: The cause of decreased pan evaporation over the past 50 years. *Science*, 298, 1410–1411.
- Schaake, J. C., V. I. Koren, Q.-Y. Duan, K. Mitchell, F. Chen, 1996: Simple water balance model for estimating runoff at different spatial and temporal scales. *Journal of Geophysical Research*, 101 (D3), 7461–7475.
- Schimel, D.S., B.H. Braswell, W.J. Parton, 1997: Equilibration of the terrestrial water, nitrogen, and carbon cycles. *Proceedings of the National Academy of Sciences of the United States of America*, 94(16), 8280–8283.

- Sillmann, J., V. V. Kharin, X. Zhang, F. W. Zwiers, and D. Bronaugh, 2013: Climate extremes indices in the CMIP5 multimodel ensemble: Part 1. Model evaluation in the present climate. *Journal of Geophysical Research: Atmospheres*, 118, 1–18.
- Skamarock, W. C., J. B. Klemp, J. Dudhia, D. O. Gill, D. M. Barker, M. G. Duda, X-Y. Huang, W. Wang and J. G. Powers, 2008: A Description of the Advanced Research WRF Version 3, NCAR Technical Note, NCAR/TN-475+STR, 123 pp. Available on-line at: http://www.mmm.ucar.edu/wrf/users/docs/arw_v3.pdf
- Slack, J. R., A. M. Lumb, J. M. Landwehr, 1993: U.S. Geological Survey Hydro-Climatic Data Network (HCDN): Streamflow Data Set, 1874 - 1988, USGS Water-Resources Investigations Report 93-4076, <http://water.usgs.gov/pubs/wri/wri934076/>.
- Stewart, I., D.R. Cayan, and M.D. Dettinger, 2004: Change in snowmelt runoff timing in western North America under a “Business as Usual” climate change Scenario. *Climatic Change*, 62, 217–232
- Taylor, K. E., R. J. Stouffer, G. A. Meehl, 2012: An overview of CMIP5 and the experiment design. *Bulletin of the American Meteorological Society*, 93, 485–498.
- Trenberth, K.E., P.D. Jones, P. Ambenje, R. Bojariu et al., 2007: Observations: surface and atmospheric climate change. *Climate Change 2007: The Physical Science Basis. Contribution of Working Group I to the Fourth Assessment Report of the Intergovernmental Panel on Climate Change*, S. Solomon, D. Qin, and M. Manning, Eds., Cambridge University Press, Cambridge and New York, 996pp.
- U.S. Metro Economies -- Gross Metropolitan Product with Housing Update, 2007: The United States Conference of Mayors and The Council for the New American City. Global Insight, Inc

- U. S. Global Change Research Program (2009) Global climate change impacts in the United States. In: Karl RT, Melillo JM, Peterson TC (eds) Cambridge University Press, New York.
<http://www.globalchange.gov/publications/reports/scientific-assessments/usimpacts>
- Wang Y., L.R. Leung, J.L. McGregor, D.K. Lee, W.C. Wang, Y. Ding , F. Kimura, 2004:
Regional climate modeling: progress, challenges, and prospects. Journal of the Meteorological Society of Japan, 82, 1599-1628.
- Wang, Z., X. Zeng, 2010: Evaluation of Snow Albedo in Land Models for Weather and Climate Studies, Journal of Applied Meteorology and Climatology, 49, 363-380.